University of Alberta

Library Release Form

Name of Author: Greg Altimas

Title of Capstone Project: Evaluation of local kinematics of atmospheric vortex flows

Degree: Master of Engineering

Year this Degree Granted: 2007

. . . . . .

Greg Altimas
4-9 Mechanical Eng. Bldg.
University of Alberta
Edmonton, AB T6G 2G8

Date: . . . . . .

Evaluation of local kinematics of atmospheric vortex flows

August 2007

by

Greg Altimas

University of Alberta

Evaluation of local kinematics of atmospheric vortex flows

by

Greg Altimas

A report submitted to the Faculty of Graduate Studies and Research in partial fulfillment of the requirements for the degree of Master of Engineering

Department of Mechanical Engineering

Edmonton, Alberta
Fall 2007

University of Alberta

Faculty of Graduate Studies and Research

The undersigned certify that they have read, and recommend to the Faculty of Graduate Studies and Research for acceptance, a report entitled **Evaluation of local kinematics of atmospheric vortex flows** submitted by **Greg Altimas** in partial fulfillment of the requirements for the degree of **Master of Engineering**.

. . . . . .
Dr. Carlos F. Lange (Supervisor)

. . . . . .
Dr. Warren H. Finlay (Reviewer)

. . . . . .
Dr. André G. McDonald (Reviewer)

Date: . . . . . .

To my wife

Abstract

The present study investigates ways to simulate laboratory scale dust devils subject to Earth's ambient conditions. Numerical models similar to Gallus et al. [2006] laboratory apparatus have been developed. This type of apparatus is desirable because it does not fix the internal structure of the vortex flow and is capable of simulating a translating atmospheric vortex. A sensitivity study was conducted to investigate flow response to key apparatus geometric parameters. Results from the sensitivity study provide design input for a laboratory apparatus capable of generating a wide range of vortex flows that will function within geometric restrictions of existing experimental facilities. A method is provided for determining the vortex center location using the velocity magnitude. Numerical models are validated by comparing previous experimental and numerical results to numerical simulation results generated for this study. The numerical results from this study can be compared to experimental results as part of future work. The primary conclusions are: 1) the Gallus type apparatus can generate flows representative of atmospheric vortex flows; 2) the RSM-SGG model is in better agreement with published experimental data than the k-ε model, despite still exhibiting artificial diffusion; and 3) a single velocity and length scale defined at the core radius can adequately characterize important vortex core flow features for a wide range of vortex flow configurations.

Acknowledgements

I would like to thank my supervisor Dr. Carlos F. Lange for his dedication and continuous support that helped me to complete this study.

Secondly, I would like to extend my sincerest thanks to post-doctoral fellow Dr. Jeff Davis for his contributions during the project and for his assistance with initial model development.

I would also like to thank Luis Prieto for his previous efforts in the study of atmospheric vortex flows.

I acknowledge the financial support from the Canadian Space Agency.

Contents

List of Tables

List of Figures

List of Symbols

a = aspect ratio
C = dimensionaless constant of proportionality
$C_{\varepsilon 1}$ = $k-\varepsilon$ model constant
$C_{\varepsilon 2}$ = $k-\varepsilon$ model constant
C_{μ} = $k-\varepsilon$ model constant
h = depth of the inflow layer, m
k = turbulence kinetic energy, $\mathrm{m}^2/\mathrm{s}^2$
L^* = dimension scale, m
Q = volume flow rate, m^3/s
p = pressure of the fluid, Pa
P_k = Turbulence production component in the $k-\varepsilon$ model p_0 = standard atmospheric pressure, 101,325 Pa
Re = Reynolds number
r = radius, m
S_i = additional momentum sources in the i direction
S_0 = swirl ratio defined at updraft hole
S_{core} = swirl ratio defined at vortex core
t = time, s
U_r = radial velocity, m/s
U_θ = tangential velocity, m/s
U_z = axial velocity, m/s
U = time averaged velocity, m/s
$\mathbf{u}$ = velocity field (vector) of the fluid, m/s
u_i, u_j, u_k = velocity component in the index notation, m/s
u_i', u_j', u_k' = time-varying fluctuating velocity component in the index notation, m/s
V^* = velocity scale, m/s

Greek symbols
δ = Krnonecker delta function
Γ_{core} = circulation at vortex core, m^2/s
θ = Fin angle, angle downdraft is turned from vertical, $^\circ$
μ = dynamic viscosity, Pa·s
μ_t = eddy viscosity, Pa.s
Φ = turbulent scalar quantity of the fluid
Ψ_{ij} = quadratic pressure-strain correlation, $\mathrm{kg/m{\cdot}s}^3$

ϕ = scalar quantity of the fluid
τ = molecular stress tensor ρ = total density of the fluid, kg/m^3
ρ_a = air density, kg/m^3
$\sigma_k = k - \varepsilon$ model constant
$\sigma_\varepsilon = k - \varepsilon$ model constant
Υ_{ij} = shear turbulence production, kg/m·s^3
ε = turbulence dissipation rate, m^2/s^3

Subscripts
$_r$ = radial direction
$_\nu$ = tangential direction at location of maximum tangential velocity
$_0$ =location of updraft hole of a Ward's type apparatus
$_{center}$ = location of vortex center
$_{core}$ = location of maximum tangential velocity

System of coordinates
x, y, z = Cartesian system
r, θ, z = cylindrical system
i, j, k = index notation

Overbar
- = time-averaged

Chapter 1

Introduction

Mars exploration has revealed evidence on the past and present cycle of water. The presence of water on Mars provides a compelling reason to continue planetary exploration as water has been identified as a key component to sustaining life. It is believed that there is significant movement of water that is linked to a complex meteorological system. Recent studies, such as Zhao et al. [2004], have shown that thermal gradients can concentrate ambient vorticity to form a highly swirling flow with a low pressure core, that are similar to dust devils observed on Earth. It is believed that an apparent high occurrence of dust devils on Mars (Thomas and Gierasch [1985], Metzger et al. [1999]) could potentially affect the mass transport of water. A detailed evaluation of these atmospheric vortex flows can improve our understanding of the movement of water throughout the Martian environment.

The Phoenix Mars Mission has been designed to search for evidence of life and to study the mass transport of water near the landing site. One of the objectives of the Phoenix Mars Mission will be to study the mass transport of water vapour in the vicinity of the lander. However, meteorological instrumentation will record only a fraction of the necessary measurements. Furthermore, the lander itself will influence the local flow patterns. Thus, the meteorological measurements alone will not be sufficient to provide the evidence necessary to meet the Mission's objectives. A numerical model of the flow around the lander can be used to interprete the measured data, as well as derive quantities that cannot be measured directly such as the water vapour flux.

The Martian climate can be simplified into four basic conditions: 1) calm air; 2) horizontal crosswind; 3) free convection plumes; and 4) atmospheric vortex (dust devil). The University of Alberta is involved in developing numerical models that capture these basic flow conditions with the objective of developing an understanding of how each of these flows influence the mass transport of water vapour through the Martian regolith, as the soil in Mars is called for consisting of a layer of loose heterogeneous material resting on solid rock.

A previous study conducted at the University of Alberta (Prieto [2006]) has developed numerical models to assess the mass transport of water in calm air, horizontal crosswind and atmospheric vortex. This previous study considered flows subject to Earth's ambient conditions, because numerical and laboratory model development is much more cost effective using Earth's atmosphere. Furthermore, documented results from previous observations of naturally occurring atmospheric flows, as well as previous numerical studies contributed to model development efforts. The considered flows were simulated numerically in a manner that could be readily developed into an experimental test apparatus. Laboratory experiments can then be used to validate the numerical model results. This previous study uncovered several short comings in the selected vortex generator and the present investigation attempts to address these issues by numerically evaluating a vortex generator based on a more robust design developed by Gallus et al. [2006].

Physical testing is relatively limited in providing sensitivity information because of difficulties in parametric control and cost limitations. The present study focuses on the development of numerical models of vortex flows subjected to Earth's ambient conditions. The numerical simulation results are validated using results from previous studies. To develop reliable numerical representations further numerical model validation is planned in future studies using test results obtained from a dedicated experimental facility. Findings from this study will contribute to the design of an improved laboratory apparatus. The objectives of this investigation include: 1) a sensitivity study using a computationally efficient numerical model to investigate the optimum apparatus geometry; 2) an evaluation of a three-dimensional numerical model using available turbulence models, the $\kappa - \epsilon$ model and the Reynolds Stress Model (RSM); and 3) a three-dimensional numerical model used to investigate parameters that can be used to characterize the local vortex kinematics. The numerical model development performed in this study will aid future studies aimed at char-

acterizing vortex flows in a Martian environment and investigating the vortex flow influence on the mass transport of water through the Martian regolith.

Chapter 2

Background

2.1 Discussion on Vortex Generators

Previous reviews on laboratory vortex generating apparatus, such as Davies-Jones [1976] and Church and Snow [1993], have indicated that the Ward-type generator, developed by Ward [1972] (Figure 2.1), can adequately simulate a vortex core flow in the laboratory environment. This apparatus is not appropriate for the current study because it does not allow translation of the swirling flow along a surface. This method of creating the vortex (i.e. updraft hole) is undesirable because it fixes the internal vortex structure.

A previous investigation, conducted by Prieto [2006], was based on an "Open" model tornado generator, developed by Hsu [1973] and illustrated in Figure 2.2. This apparatus introduces vorticity by using an axial duct fan. The fan blades are oriented vertically in order to minimize the axial momentum imparted to the flow. Although this test apparatus could be translated laterally, it exhibited relatively weak vortices and excessive widening of the vortex core (Prieto [2006]). This type of generator did not produce the desired vorticity or kinematic characteristic, likely due to the reliance on viscous forces to produce upward angular momentum.

In Prieto's study, a numerical model representing the "Open" vortex generator was created by using a rotating wall at the top boundary to generate the vortex core flow. The numerical model exhibited the same behaviour as observed in the experimental apparatus. However,

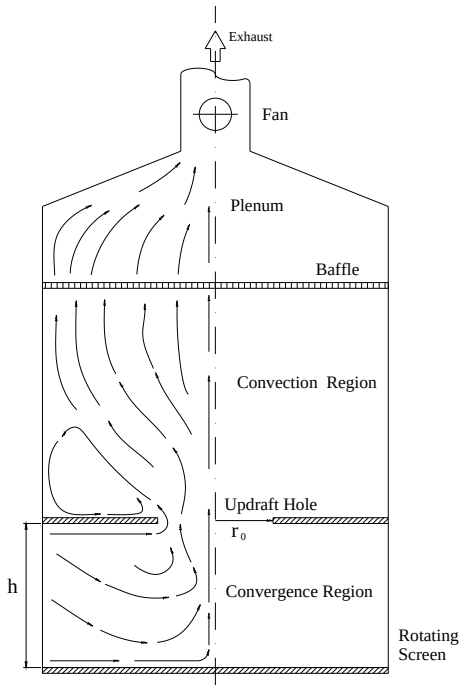

Figure 2.1: A schematic of the Ward-type vortex generator.

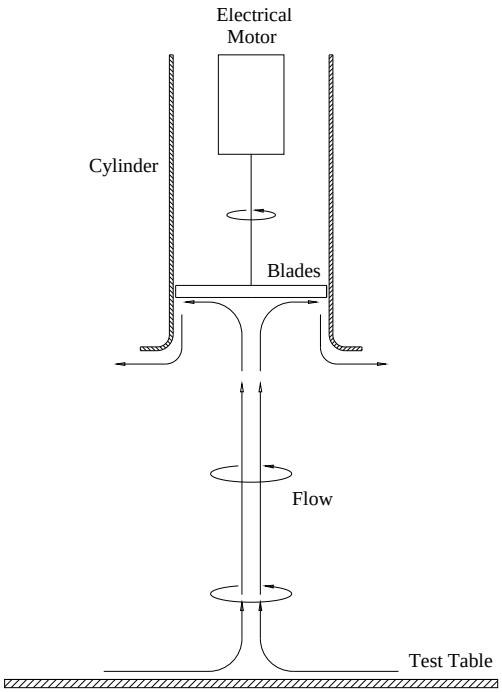

Figure 2.2: A schematic of the "Open" model vortex generator.

numerical results indicated a significantly weaker vortex flow than laboratory tests. This discrepancy may be attributed in part to the small amount of axial momentum produced by the laboratory apparatus, while the constraints of the numerical domain did not allow any axial flow at the vortex generator. Although the study of the "Open" vortex generator did not produce the desired characteristics, it did demonstrate that the atmospheric vortex can play a significant role in water transport and it also emphasized the need to include axial forcing to maintain a narrow vortex core flow.

Researchers have concluded that two necessary conditions must exist for the formation of atmospheric vortices: 1) axial forcing or updraft; and 2) presence of an initial tangential velocity (Howells et al. [1988]). The vortex generator developed at Iowa State University by Gallus et al. [2006] exhibits the mentioned characteristics, as well as allows for lateral translation (illustrated in Figure 2.3). Although similar in function to the Ward vortex generator, this test apparatus does not fix the internal structure of the vortex. This apparatus simulates the inflow layer by redirecting the axial momentum, introduced by an axial fan, through ducts and introduces tangential velocity through the use of fins spaced evenly around the circumference.

2.2 Kinematic Similarity

This study is primarily concerned with the local kinematics of simulated atmospheric vortex flows. In nature, there is a wide range of kinematics observed depending on the boundary conditions sustaining the swirling flow. Furthermore, formation of several kinematic structures can occur as the vortex progresses through various stages of development. The vortex core kinematic structures observed in nature are thoroughly described in Snow [1982] and Church and Snow [1993].

The precise definition of the dimensionless parameters used to characterize vortex flow is not well established for transient and highly unstable three-dimensional vortices. However, researchers generally agree that a steady state, incompressible, axisymmetric vortex flow in a closed cylinder can be characterized by three dimensionless parameters: a radial Reynolds

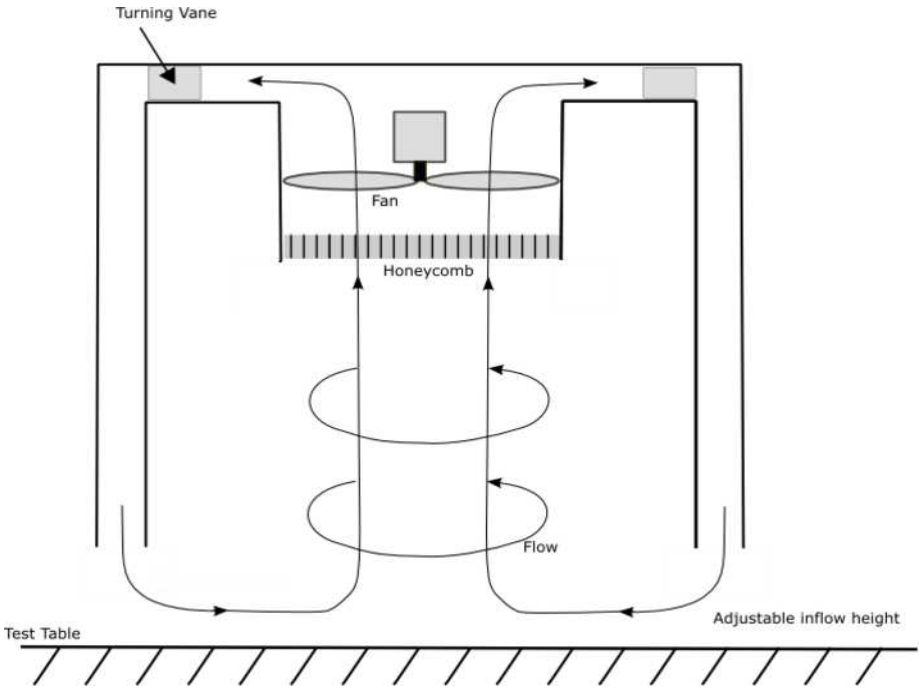

Figure 2.3: A schematic of vortex generator developed by Gallus et al. [2006].

number, Re_r, a swirl ratio, S_0, and an aspect ratio, a_o, (Lewellen [1962]and Davies-Jones [1973]) defined respectively as

$$\mathrm{Re}_r = \frac{\rho\, r_0\, U_r}{\mu} \tag{2.1}$$

$$S_0 = \frac{r_0\, U_\theta}{2hU_r} \tag{2.2}$$

$$a_0 = \frac{h}{r_0} \tag{2.3}$$

where r_0 is the radius of updraft (location of maximum radial velocity), h the depth of inflow (as shown in Figure 2.1), U_θ is the mean tangential velocity, U_r is the mean radial velocity (U_θ and U_r are measured at r_0), ρ is the mass density and μ is the dynamic viscosity. These parameters work well for a Ward type generator where the kinematic structure of the vortex core is fixed by the chamber's geometry. However, the present investigation requires an internal vortex structure that can vary depending on external flow conditions, as well as the ability to translate along the lower bounding surface.

In these situations, some researchers including Prieto [2006] and Rotunno [1979] continue to define dimensionless parameters at the radial location of the maximum radial velocity. However, studies such as Lewellen and Lewellen [2000] argue that the location of maximum tangential velocity, or core radius, r_{core}, is a more suitable location to characterize the internal vortex structure. The present investigation defines dimensionless parameters using the core radius as:

$$\Gamma_{core} = 2\,\Pi\, r_{core}\, U_{core} \tag{2.4}$$

$$Re_{core} = \frac{\Gamma_{core}}{\nu} \tag{2.5}$$

$$S_{core} = \frac{r_{core}\Gamma_{core}}{2Q} \tag{2.6}$$

$$a_{core} = \frac{h_{core}}{r_{core}} \tag{2.7}$$

where Γ_{core} is defined as the circulation at the core radius, U_{core} is the average tangential velocity at r_{core}, Q is the volume flow rate and ν the kinematic viscosity. The above parameters are used for characterizing the quasi-steady circumferentially periodic numerical model used in the sensitivity study. However, it is likely that the nature of three-dimensional vortex flows will render the mentioned characterization inadequate. The parameters used to characterize the vortex flow will be re-assessed in the evaluation of the three-dimensional numerical model.

The swirl ratio provides an indication of vortex strength and is defined as the ratio of angular momentum to axial momentum. Previous laboratory and numerical modeling show the swirl ratio strongly governs the vortex flow, while Church et al. [1979] found that, for smooth surfaces, the internal vortex structure exhibits weak dependence on the aspect ratio and on large values of Reynolds. Although it is known that a single dimensionless ratio is inadequate to fully characterize a vortex flow, it has been shown that, in some cases, it can adequately assess a wide range of vortex flows (Lewellen and Lewellen [1997]).

2.3 Existing Experimental Facility

In previous work at the University of Alberta (Prieto [2006]) several experimental apparatuses were designed to determine the mass transport of water through a porous medium under several flow conditions. In this section, a brief overview of the facility and apparatus used for evaluating atmospheric vortex flows is provided for convenience, as information in this section was originally documented in Prieto [2006].

The experimental facilities are currently housed in a semi-closed environment illustrated in Figure 2.4, which consists of a 6.05 m x 3.54 m x 3.40 m room. The room presents a quasi-steady air circulation due to the presence of three inflow zones (blue area), and one outlet zone (red area). Results from Prieto [2006] show that room air circulation does not significantly affect the vortex flow.

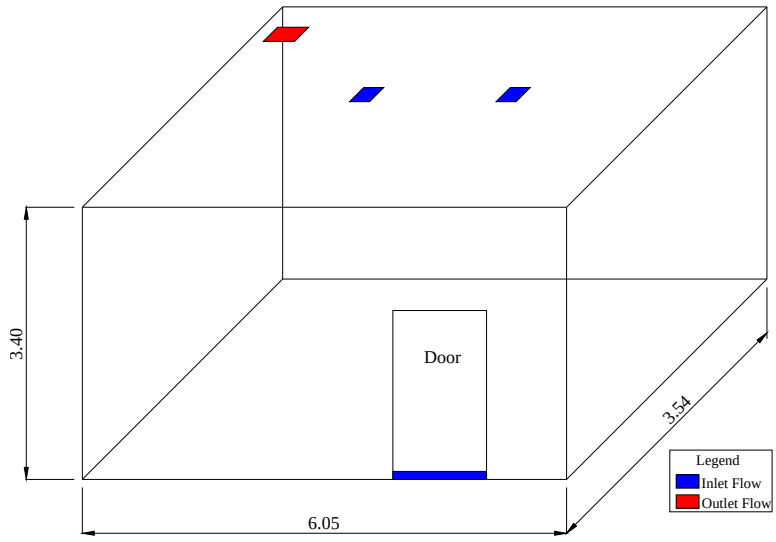

Figure 2.4: Schematic of the laboratory environment

The "Open" vortex generator used in Prieto [2006] is similar to the one used by Greeley et al. [2001], and it is shown in Figure 2.5. The vortex generator consists of a support frame, an axial duct fan, and a test table. The axial duct fan includes a cylinder, 0.45 m in diameter, a motor drive with variable speed, and a four-blade fan system at 90 degrees to each other. This arrangement is mounted to the frame, so that future applications will

allow translation of the cylinder along the test table to simulate motion of the vortex across the terrain. The table is 2 m x 1 m, and it is detached from the frame to avoid potential motor vibrations. The new vortex generator should take advantage of existing equipment, where possible.

Figure 2.5: The "Open" vortex generator device showing the axial duct fan, the frame, and test table.

Chapter 3

Theory

3.1 Governing Equations

This study only considers Earth's ambient conditions and, as a consequence, the continuum assumption is valid. This assumption should be questioned in future studies when the atmospheric pressure on Mars is considered. The continuum assumption allows the Navier-Stokes equations to be used to solve for the velocity and pressure fields of a compressible Newtonian fluid. The Navier-stokes equations can be simplified because flow model simplifications can be justified including: 1) a constant fluid density because maximum fluid velocities are well below the speed of sound (i.e. incompressible flow); and 2) an isothermal assumption is justified because the flow kinematics is the primary focus of this analysis and, consequently the effect of gravity can also be neglected. The Navier-stokes relations considered for this study includes:

- Conservation of Mass:

$$\frac{\partial \rho}{\partial t} + \nabla \cdot (\rho \mathbf{u}) = 0 \tag{3.1}$$

- Conservation of Momentum:

$$\frac{\partial \rho u_i}{\partial t} + \nabla \cdot (\rho u_i \mathbf{u}) = -\nabla p + \nabla \cdot \tau + S_i \tag{3.2}$$

- Viscous stress tensor, τ:

$$\tau = \mu(\nabla \mathbf{u} + (\nabla \mathbf{u})^T) \tag{3.3}$$

Turbulence generates a continuous distribution of velocity fluctuations (i.e. eddies) and is a highly non-linear irrevisible phenomenon strongly governed by the mean flow. Turbulence always appears when the Reynolds number is sufficiently high. Therefore, the effects of turbulence on the flows considered in this study are expected to be considerable, since flows considered in this study have Re on the order of 10^5. The Navier-Stokes equations are believed to accurately describe turbulent motion. However, it is not feasible to directly simulate turbulence due to vast computational resources required for this type of analysis. A number of computationally efficient turbulence models have been developed. Turbulence models introduce a significant loss of flow information and are a large source of error. However, they have been proven to provide useful engineering approximations for a large range of flow configurations.

To date, the most widely used turbulence models are based on statistical ensemble averaging. Transport variables (i.e., velocity, pressure, etc.) are decomposed into the statistical mean and turbulent fluctuations. For instance, $\mathbf{u} = \mathbf{U} + \mathbf{u'}$, where, $\mathbf{u}$ is the instantaneous velocity, $\mathbf{U}$ is the time averaged velocity, and $\mathbf{u'}$ is the time-varying fluctuating velocity component. As a result of this simplification, time averaged turbulent models are not able to capture large scale turbulent structures. The Reynolds Averaged Navier Stokes (RANS) equations are derived by applying ensemble averaging to the Navier Stokes equations. The averaged fluctuating component adds a second order effect, $\mathbf{u'} \approx 0$ but $\mathbf{u'u'} \neq 0$, because of this fluctuating terms appear only in the momentum equation:

- RANS Conservation of Momentum:

$$\frac{\partial \rho U_i}{\partial t} + \nabla \cdot (\rho U_i \mathbf{U}) = -\nabla P + \nabla \cdot (\tau - \rho u_i \mathbf{'u'}) + S_i \tag{3.4}$$

The fluctuating component, $\rho u_i \mathbf{'u'}$, causes additional stresses refered to as Reynolds stresses. The Reynolds stresses produce a system with more unknowns than equations (The Closure Problem). Turbulence models employ further simplifications to close these equations. A commmon approach is based on the concepts of gradient-diffusion and turbulent viscosity (also called eddy viscosity), μ_t, where the Reynolds stresses are related to the mean velocity gradients, using a direct analogy to the viscous stress in a Newtonian fluid (molecular stress tensor). The Reynolds stress terms are modelled as:

$$-\rho u_i\text{'}\mathbf{u}\text{'} = \mu_t \left(\nabla \mathbf{U} + (\nabla \mathbf{U})^T\right) - \frac{2}{3}\rho k \delta \tag{3.5}$$

The $k-\varepsilon$ model originally developed by Launder and Spalding [1974] has been chosen for the sensitivity study conducted as part of this investigation, due to low costs in terms of computing resources, and because it is the most validated turbulence model. This two-equation turbulence model is based on the assumption that the eddy viscosity through dimensional analysis can be characterized by turbulence kinetic energy, k, a length scale, L, and C a constant of proportionality.

$$\mu_t = C\rho k^{1/2} L \tag{3.6}$$

The turbulence energy dissipation rate, ε, can be related to the length character and the kinetic energy of turbulence using the following relationship (i.e. assumes equilibrium turbulent flow or, flow in which the rates of production and destruction of turbulence are in near balance [Kolmogorov, 1941]).

$$\varepsilon \approx \frac{k^{3/2}}{L} \tag{3.7}$$

The standard $k-\varepsilon$ model for a transient Newtonian compressible flow developed by Launder and Spalding [1974] requires solving two additional transport equations:

$$\frac{\partial(\rho k)}{\partial t} + \nabla \cdot (\rho k \mathbf{U}) = \nabla \cdot \left[(\mu + \frac{\mu_t}{\sigma_k})\nabla k\right] + P_k - \rho\varepsilon \tag{3.8}$$

$$\frac{\partial(\rho \varepsilon)}{\partial t} + \nabla \cdot (\rho \varepsilon \mathbf{U}) = \nabla \cdot \left[(\mu + \frac{\mu_t}{\sigma_\varepsilon})\nabla \varepsilon\right] + \frac{\varepsilon}{k}(C_{\varepsilon 1} P_k - C_{\varepsilon 2}\rho\varepsilon) \tag{3.9}$$

Where P_k is the turbulence production due to viscous forces consisting of:

$$P_k = \mu_t \nabla \mathbf{U} \cdot (\nabla \mathbf{U} + (\nabla \mathbf{U})^T) \tag{3.10}$$

and turbulent viscosity as

$$\mu_t = C_\mu\ \rho k^2/\varepsilon \tag{3.11}$$

The $k-\varepsilon$ model contains five parameters. This study employs the most commonly used values for them consisting of: $C_\mu = 0.09$; $C_{\varepsilon 1} = 1.44$; $C_{\varepsilon 2}$= 1.92; $\sigma_k = 1$; $\sigma_\varepsilon = 1.3$.

The $k-\varepsilon$ turbulence model exhibits deficiencies from the assumption that the Reynolds stresses are proportional to the mean rate of strain and from the equilibrium turbulent

flow assumption. Another statistically time averaged turbulence model more suitable for representing rotating flow is the Reynolds Stress Model (RSM). The RSM model solves transport equations for individual Reynolds Stresses and for the dissipation (ε) making this model more costly. However, directly representing the Reynolds-stresses allows the RSM model to be successful (whereas the $k-\varepsilon$ model is not) in calculating flows with significant mean streamline curvature, strongly rotating flow, secondary flows in ducts, and flows with rapid variations in the mean flow (Pope [2000]). Prieto [2006] identified that the $\kappa-\varepsilon$ turbulence model exhibits excessive production of turbulent kinetic energy near areas of large velocity gradients by comparing $\kappa-\varepsilon$ and RSM turbulence models with experimental data using a numerical representation of a Ward type apparatus.

The transport of Reynolds stresses is balanced by four processes - production (Υ), dissipation (ε), redistribution Ψ, and turbulent transport. The first three processes are dominant and comparable (Pope [2000]). The production is in closed form, for large Reynolds numbers the dissipation is well represented using an isotropic formulation, leaving the redistribution due to the fluctuating pressure field, Ψ pressure-strain tensor, as the principal component to be modelled. Generally, RSM models assume that terms being modelled are independent of the Reynolds number and that turbulence is homogenous (i.e. the fluctuating velocity is statistically homogeneous). This study uses the RSM model developed by Speziale et al. [1991] (RSM-SSG) because the quadratic pressure-strain correlation used in this model has been found to be more representative for swirling flows than other RSM versions, which use a linear relation for the pressure-strain correlation such as the earlier model developed by B. E Launder and Rodi [1975]. The RSM-SGG Reynolds stress transport equation is given by

$$\frac{\partial\left(\rho u_i' u_j'\right)}{\partial t}+\frac{\partial\left(u_k \rho u_i' u_j'\right)}{\partial x_k}=\frac{\partial}{\partial x_k}\left[\left(\mu\delta_{kl}+C_S\rho\frac{k}{\varepsilon}u_k' u_l'\right)\frac{\partial u_i' u_j'}{\partial x_l}\right] -\frac{2}{3}\delta_{ij}\rho\varepsilon+\Upsilon_{ij}+\Psi_{ij} \tag{3.12}$$

Where Υ_{ij} is the shear turbulence production:

$$\Upsilon_{ij} = -\rho \left[u_i' u_j' \left(\nabla \mathbf{U} \right)^T + \left(\nabla \mathbf{U} \right) u_i' u_j' \right] \tag{3.13}$$

The turbulence energy dissipation is modeled using an isotropic formulation for the diffusion coefficients:

$$\frac{\partial(\rho\varepsilon)}{\partial t} + \frac{\partial \left(\rho U_k \varepsilon \right)}{\partial x_k} = \frac{\varepsilon}{k}(C_{\varepsilon 1}\Upsilon - C_{\varepsilon 2}\rho\varepsilon) + \frac{\partial}{\partial x_k}\left[\left(\mu + \frac{\mu_t}{\sigma_k} \right) \frac{\partial \varepsilon}{\partial x_k} \right] \tag{3.14}$$

As discussed previously, the most important term in RSM models is the pressure-strain tensor, Ψ_{ij}, expressed in general form:

$$\Psi_{ij} = \Psi_{ij1} + \Psi_{ij2} \tag{3.15}$$

where:

$\Psi_{ij1} = -\rho\varepsilon(C_{s1}\mathbf{a} + C_{s2}(\mathbf{aa} - \frac{1}{3}\mathbf{a}\cdot\mathbf{a}\delta))$
$\Psi_{ij2} = -C_{r1}\Upsilon\mathbf{a} + C_{r2}\rho k\mathbf{S} - C_{r3}\rho k\mathbf{S}\sqrt{\mathbf{a}\cdot\mathbf{a}}$
$+ C_{r4}\rho k(\mathbf{a}\mathbf{S}^T + \mathbf{S}\mathbf{a}^T - \frac{2}{3}\mathbf{a}\cdot\mathbf{S}\delta)$
$+ C_{r5}\rho k(\mathbf{a}\mathbf{W}^T + \mathbf{W}\mathbf{a}^T)$

and:

$\mathbf{a} = \frac{u_i' u_j'}{k} - \frac{2}{3}\delta$
$\mathbf{S} = \frac{1}{2}(\nabla\mathbf{U} + (\nabla\mathbf{U})^T)$
$\mathbf{W} = \frac{1}{2}(\nabla\mathbf{U} - (\nabla\mathbf{U})^T)$

Where, $\mathbf{a}$ is the anisotropy tensor, $\mathbf{S}$ is the strain rate, and $\mathbf{W}$ is the vorticity.

The coefficient values employed in this study consists of: $C_{s1} = 1.7$; $C_{s2} = -1.05$; $C_{r1} = 0.9$; $C_{r2} = 0.8$; $C_{r3} = 0.65$; $C_{r4} = 0.625$; $C_{r5} = 0.2$
Complete details on this turbulence model can be found in Speziale et al. [1991].

3.2 Numerical Model

An important goal of this study is to investigate the range of local flow kinematics of atmospheric vortices observed in a laboratory test apparatus. The use of numerical simulations is well suited for parametric evaluation as it allows for significant flexibility in the model geometry and the external boundary conditions. Furthermore, previous research has shown that numerical model results of atmospheric vortex flows agree with experimental data (see Church and Snow [1993]). A sensitivity study was conducted (discussed in Chapter 4) to evaluate the range of internal vortex kinematics that can be generated from a vortex generator developed to function within the geometric constraints of the existing test facility.

The simulations were performed using a second order backward Euler discretization scheme for the transient terms and a "High Resolution" scheme for the advection terms. A suitable timestep was selected to provide a computationally efficient solution while avoiding excessively high Courant numbers. The Courant number describes the relationship between the fluid speed and mesh size. For a one-dimensional grid it is defined by:

$$Courant = \frac{u\Delta t}{\Delta x} \tag{3.16}$$

where Δt is the timestep and Δx is the mesh size. A Courant number near one may be neccessary to accurately resolve transient aspects of the flow. The standard atmospheric air simulated was simplified by assuming an isothermal, incompressible, Newtonian fluid with constant fluid properties (μ=1.831e-5 kg m/s, ρ_a=1.185 kg/m^3). The mass and momentum equations were assumed to converge when the residual rms errors were less than 10^{-4}. A wedge shaped domain was employed for computational efficiency. A more representative three-dimensional model will be used to assess the appropriateness of the $\kappa - \varepsilon$ and RSM-SSG turbulence models later (discussed in Chapter 5).

The numerical simulations used an unstructured tetrahedral mesh created using the mesh generation tool "CFX-Mesh" (ANSYS Inc, Pennsylvania, US). Mesh controls were implemented to refine the mesh, where required, for solution accuracy and convergence. Figure 3.1 shows the model domain and a typical mesh used for the wedge domain model. A mesh sensitivity was performed on the baseline configuration to provide indication of the spatial discretization error. The swirl ratio and core radius at an elevation of 0.3 m is plotted as a

function of the number of nodes for five grid levels in Figure 3.2. Numerical models used in this study are spatially discretized to provide a mesh density similar to the 30850 node configuration denoted in Figure 3.2 by the vertical line. It should be noted that the mesh size chosen for this sensitivity study gives up solution accuracy for computational efficiency as the mesh sensitivity results indicate that further grid refinement is required before convergence of discretization error is obtained. The relative discretization error is determined using results for the finest mesh and the result exhibiting the largest variation within the range of mesh density of interest. For the chosen mesh size a conservative estimate of the relative discretization error in the swirl ratio due to non-converged grids is $\pm 10\%$. The results show the core radius is not as sensitive to non-converged grids, a $\pm 4\%$ discretization error is estimated. The numerical error introduced from the chosen modeling strategy is acceptable because this sensitivity study is primarily concerned with trends in the bulk flow.

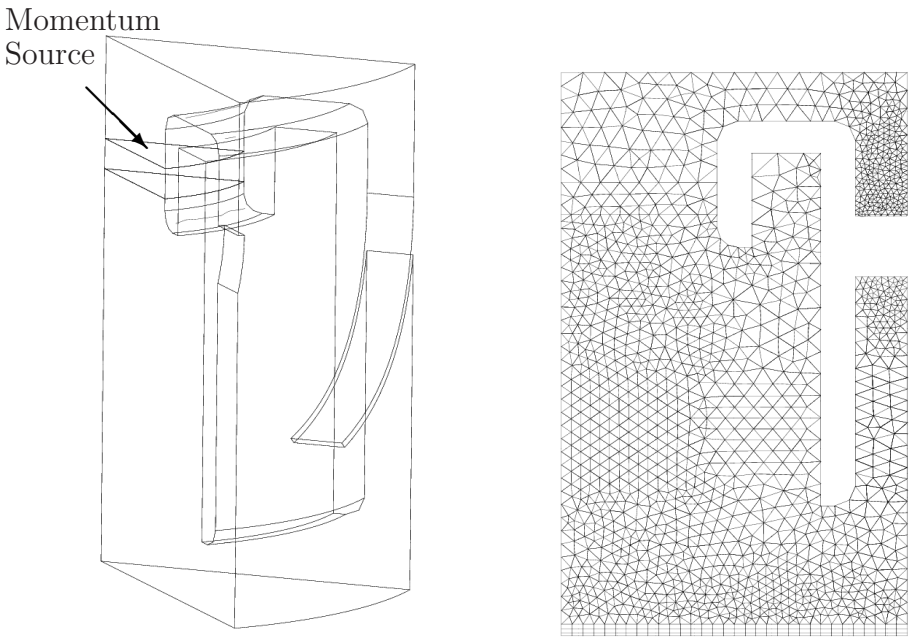

Figure 3.1: Isometric view of the wedge shaped domain modeled and a 2D slice of a typical mesh.

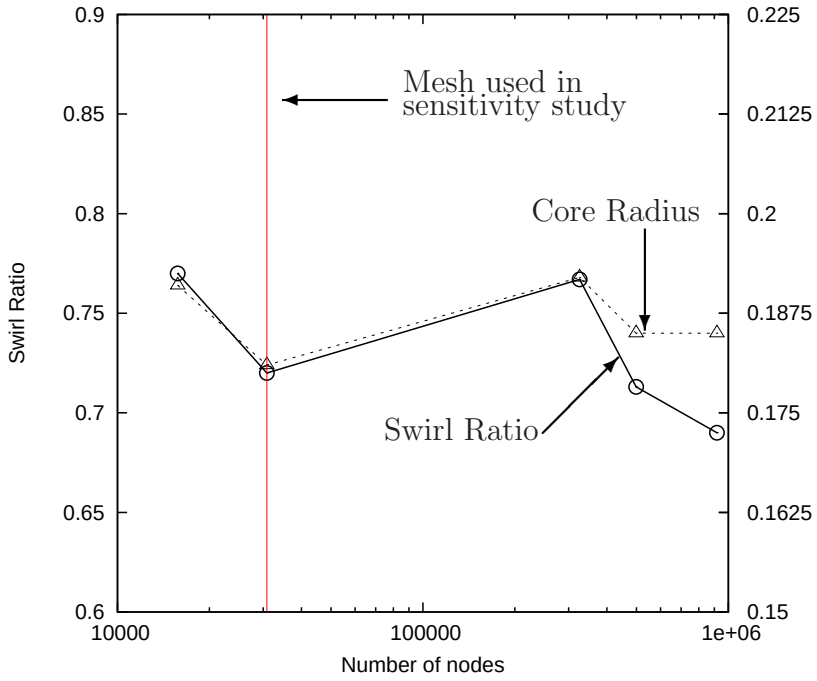

Figure 3.2: Swirl ratio and core radius at a height of 0.3 m as a function the number of nodes.

Axial momentum is introduced at the top. This section is also used to represent a honeycomb by adding a large resistance to flow in the tangential directions. This feature is necessary in the experimental apparatus to isolate the momentum source from the vortex flow. A downdraft is simulated by redirecting axial momentum using concentric cylindrical ducts and tangential velocity is introduced using fins mounted in the outer annulus. The downdraft is redirected inwards at the lower boundary.

The duct walls are modeled using a no-slip condition. For the sensitivity study, a closed cylinder is modeled and "inlet" boundary is modeled using a free-slip wall (i.e. there is no actual inlet and all fluid is recirculated). It is important to accurately represent the laboratory apparatus geometry because this study is concerned with the sensitivity of the vortex flow subject to the variations of apparatus geometry. As a consequence an axisymmetric formulation could not be implemented and therefore periodic apparatus geometry with the circumferential pattern controlled by the fin spacing was employed for computational efficiency. Thus, periodic constraints are used at the sides to enforce symmetry. A schematic of the "Gallus" type vortex generator used in this study is illustrated in Figure

3.3. This figure also shows key geometric features. The geometry of the governing baseline configuration is provided in Table 3.1.

The atmospheric vortex flows were simulated using CFX 10.0 (ANSYS Inc, Pennsylvania, US). The flows considered in the present study are fully turbulent and, therefore, the implementation of a turbulence model is necessary (discussed in previous section). A sensitivity study analyzed the vortex flows using the $\kappa - \varepsilon$ turbulence model developed by Launder and Spalding [1974] and employed wall functions to resolve flow near the boundaries. A second turbulence model, RSM-SSG was used with a three-dimensional domain to validate the sensitivity results.

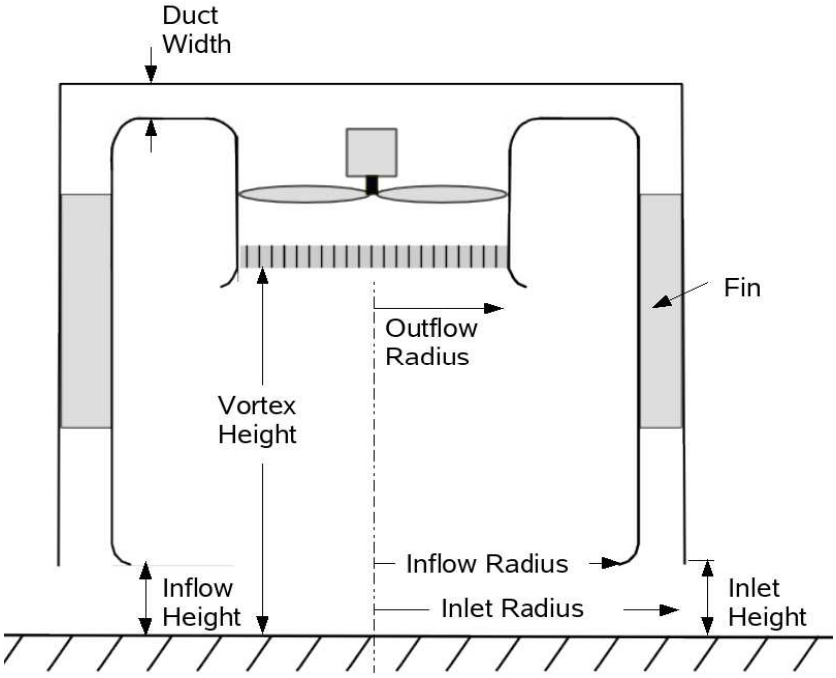

Figure 3.3: A schematic of the vortex generator showing key parameters.

The fin geometry considered in the present numerical study is illustrated in Figure 3.4. The fin angle, θ, refers to the angle between vertical and fin exit tangent and the fin ratio is defined as the fin spacing length to circumferential fin length. In this study the fin angle is varied by rotating the fin surface using a fixed radius (0.45 m). Therefore, the fin ratio changes with variation in fin angle, particularly at lower fin angles. The review by Church and Snow [1993] identified that fin geometry can have a significant influence on the vortex kinematics generated by the laboratory apparatus. Church suggested that curved vanes

are preferable to flat ones, and that the fin ratio should be near unity. A fin ratio of one represents a configuration where the downdraft area is completely covered by fin surfaces.

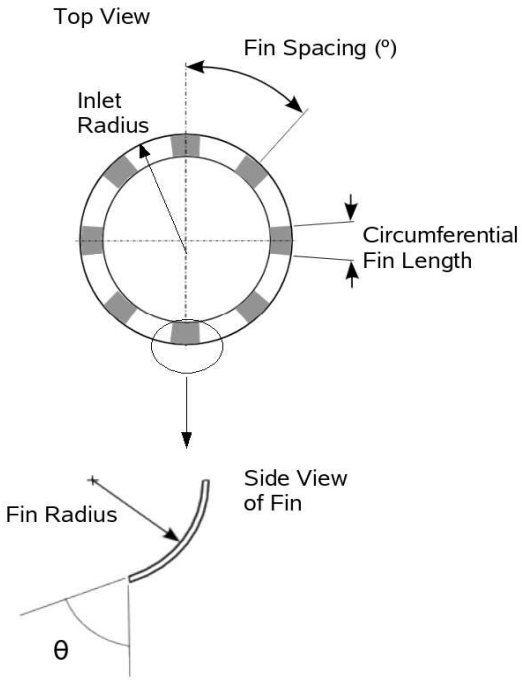

Figure 3.4: Illustration of fin geometry.

Table 3.1: Baseline geometry for wedged shaped model.

Parameter description	Value
Inlet radius	0.5 m
Inflow/Inlet height	0.115 m
Outflow radius	0.225 m
Vortex height	0.65 m
Duct width	0.075 m
Fin angle (θ)	55°
Fin spacing	45°

Chapter 4

Sensitivity Results

This chapter provides results of a sensitivity study conducted by varying each of the governing variables in Table 3.1 (presented in the Section 3.2). All flow configurations considered in this study exhibited large Reynolds numbers (i.e. Re_{core} between 20,000 and 770,000) and are expected to be fully turbulent flows. The results from this sensitivity study provide key performance characteristics required for optimizing the experimental apparatus geometry. Future studies will require a vortex generator to produce the widest range of vortex flows possible within the geometric confinements of the current experimental facility. In the later stages of this project, vortex flows over a Mars lander will be simulated at a reduced geometric scale of 1/20. As a secondary requirement, the vortex apparatus should be capable of translating over a scaled model of the Mars lander.

In the following section, the flow behavior will be interpreted primarily by the swirl ratio, since previous research has shown that vortex flows exhibit weak dependence on the aspect ratio and large Reynolds numbers (Church et al. [1979]). The results are presented at a distance above the lower boundary. Here, the vortex kinematic flow exhibits an inviscid nature and is more strongly governed by a balance between outward centrifugal forces and inward pressure forces (i.e. cyclostrophic balance). Near the lower boundary, cyclostrophic behaviour does not hold because turbulence and the boundary layer controls the vortex flow (Lewellen and Lewellen [2000]).

4.1 Flow Rate Sensitivity

Figure 4.1 shows the maximum tangential velocity and maximum radial inflow velocity as a function of the axial flow rate. The results indicate that for a given apparatus geometry the tangential velocity and radial velocity scale with the flow rate, similar to results reported in Church and Snow [1993]. The position of the core radius is governed by the balance between the outward centrifugal forces, induced primarily from tangential velocity, and the inward radial pressure force (Ward [1972]). Thus, it can be expected that the vortex kinematic structure will remain relatively constant. The swirl ratio and core radius as a function of flow rate is shown in Figure 4.2. The results show a larger variation in swirl ratio, this may be attributed in part to the greater discretization error exhibited in the swirl ratio. The relative discretization error due to non-converged grids (see Figure 3.2) is larger for the swirl ratio than core radius. In an effort to aid result interpretation, error bars showing the estimated discretization error have been included for the swirl ratio results.

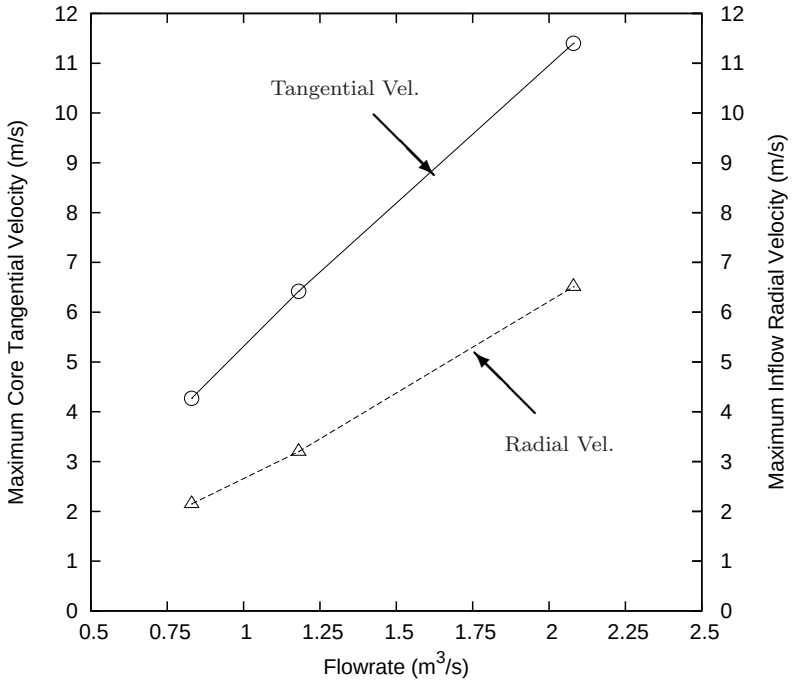

Figure 4.1: Maximum tangential velocity and inflow radial velocity as a function of the axial flow rate for baseline geometry.

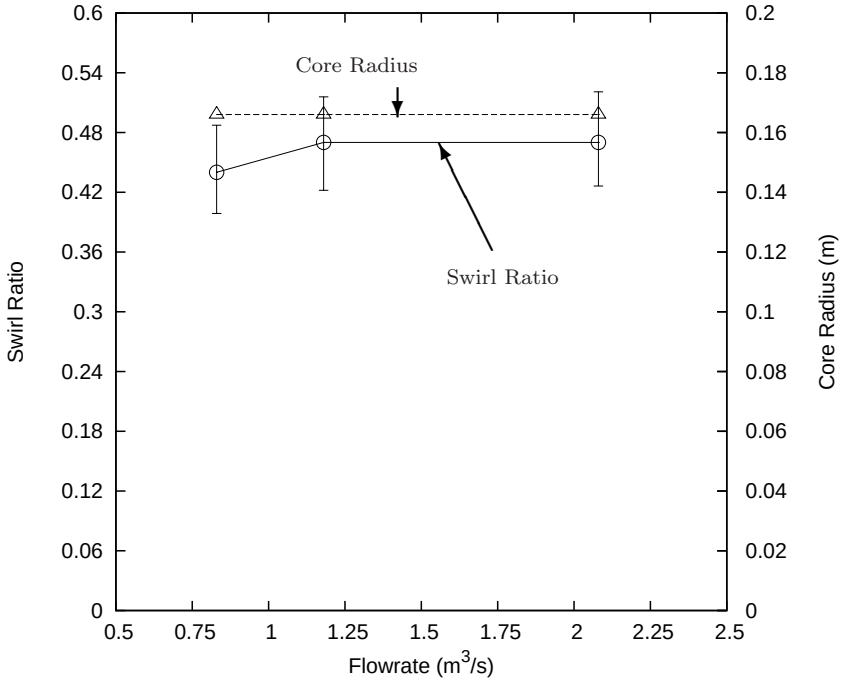

Figure 4.2: Swirl ratio (with estimated discretization error) and core radius as a function of the axial flow rate for baseline geometry, at an elevation of 0.3 m.

4.2 Initial Tangential Velocity Sensitivity

Some laboratory vortex flows are generated by supplying an initial tangential velocity (angular momentum) into an axial updraft. The convergence of far field angular momentum is an essential component of generating strong vortex flows and, it is expected that increasing the angular momentum at the inflow boundary will result in stronger generated vortex flows. Traditionally, laboratory vortex generators have employed adjustable vanes or fins to control the initial angular momentum. Figure 4.3(a) shows swirl ratio as a function of fin angle at two duct widths. These results indicate that initial angular momentum strongly governs the vortex core kinematics. These results are similar to those reported in previous experimental (Ward [1972]) and numerical (Rotunno [1977] and, Nolan and Farrell [1999]) studies. The results also show that the duct width significantly influences core structure. The baseline duct width of 0.075 m fails to produce a strong vortex core flow for fin angles below 25°, while the smaller duct width shows a smooth decline in swirl ratio up to the lowest fin angle considered. The increased vortex flow due to decreasing duct width is

attributed to the decreasing downdraft area, which results in greater tangential velocities, while the inflow radial velocity remains relatively constant.

A plot of the core radius as a function of the fin angle is shown in Figure 4.3(b). It is expected that increased angular momentum will result in a larger core radius to maintain cyclostrophic balance (Ward [1972]). Thus, an increase in the fin angle or a decrease in the duct width can be expected to result in an increase in the core radius.

It is also noted that there appears to be an abrupt change in behaviour between fin angles of 40° and 25°. Figure 4.4 shows the tangential velocity profiles at two fin angles, 40° and 25°, for the reduced duct width configuration with different curves showing variation in elevation. This result shows a significant difference in kinematics with increasing elevation for the two fin angles. With a fin angle of 40°, the vortex core flow is relatively uniform with elevation, while the configuration with a fin angle of 25° exhibits significant weakening of the vortex flow with increasing height. This is consistent with past research studies on vortex dynamics, which has identified that strong vortex flows exhibit a core radius relatively constant with increasing elevation while, moderate strength vortex flows exhibit an expansion of the core with height due to the appearance of flow instabilities (Rotunno [1979] and, Church et al. [1979]). The evolution of vortex dynamics with increasing swirl ratio has been summarized by Snow [1982]. However, the modelling strategy employed for this sensitivity study is not suitable for a detailed assessment of the dynamical behaviour.

In addition to dynamic behaviour, it is believed that the abrupt change in behaviour between fin angles of 40° and 25° can be attributed to the variations in fin ratio, as indicated through comparison of the tangential velocity profiles for the same fin angle with variation in fin ratio, presented in Figure 4.5. Church and Snow [1993] reported that fin geometry is important and an optimal vortex flow is generated when all inflow is re-directed by fin surfaces (Fin ratio = 1), as discussed in Section 3.2. In this study, the fin angle is varied while other parameters are fixed and therefore, the fin ratio varies with fin angle changes. Figure 4.6 presents variation of flow kinematics as a function of fin angle at three fin spacings for the decreased duct width configuration. These results show increasing vortex strength with decreased fin spacing. The data points provided are sufficient to show the importance of fin spacing and the trend described. Figure 4.7 shows the swirl ratio as a function of fin

ratio at two fin angles for the decreased duct width configuration. The fin ratio decribes the relationship between fin spacing and fin circumferential length and quantifies the area of downdraft not covered by fin surfaces. This result shows a decreased swirl ratio as fin ratio is increased, as expected. Results show an abrupt drop can occur at large fin ratios. However, it appears difficult to predict the thereshold fin ratio when other fin geometric parameters are varied, such as fin angle.

These results show that the initial angular momentum strongly governs the strength of the generated vortex flow and the initial angular momentum is highly sensitive to geometric parameters such as the fin spacing, duct width, and fin angle.

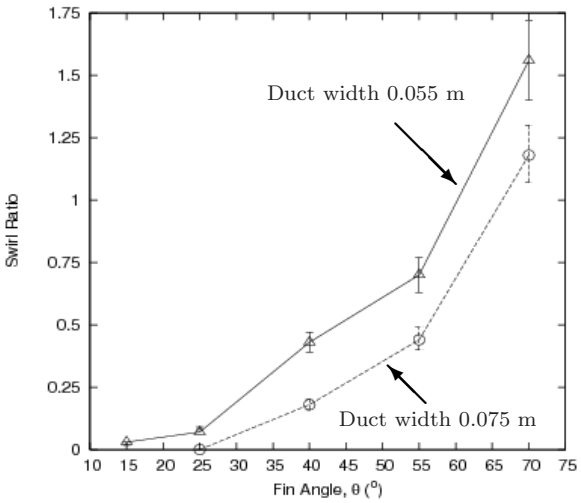

(a) Effect of swirl ratio (with estimated discretization error)

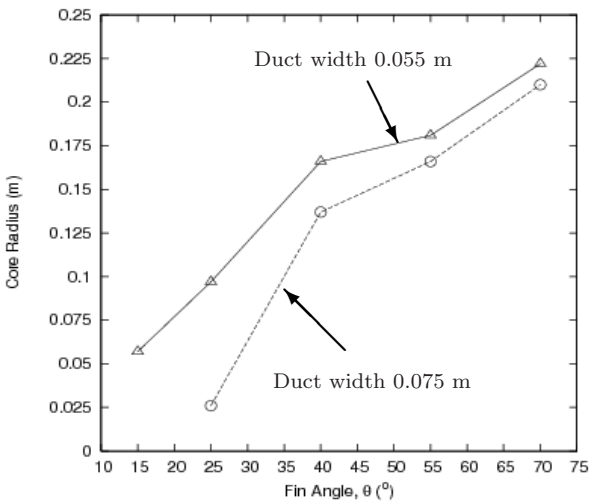

(b) Effect of core radius

Figure 4.3: Effect of the flow kinematics as a function of the fin angle for two duct widths, at an elevation of 0.3 m.

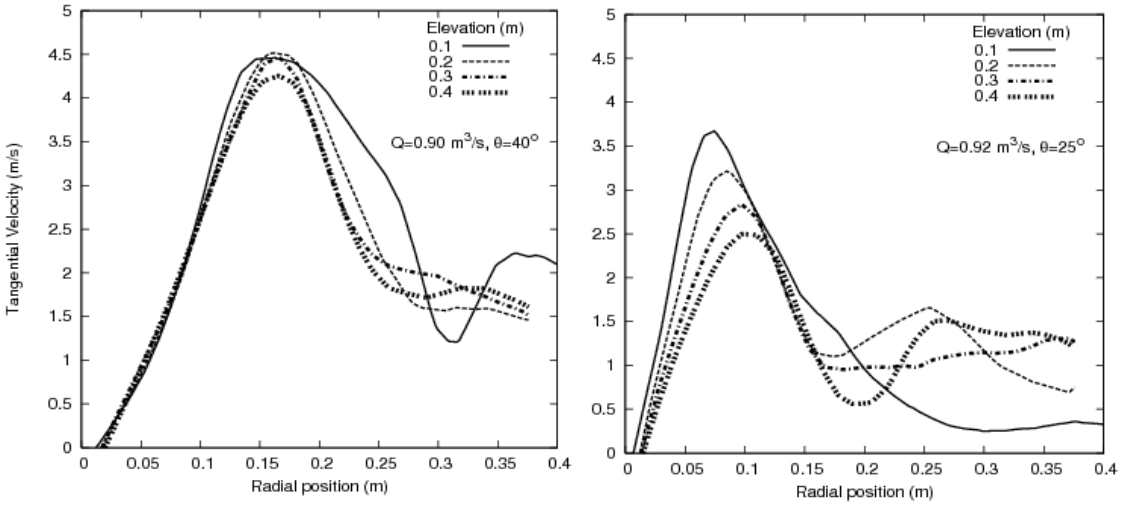

(a) fin angle 40° (b) fin angle 25°

Figure 4.4: Tangential velocity radial profiles at various elevations, for a duct width of 0.055 m and a fin spacing of 45°.

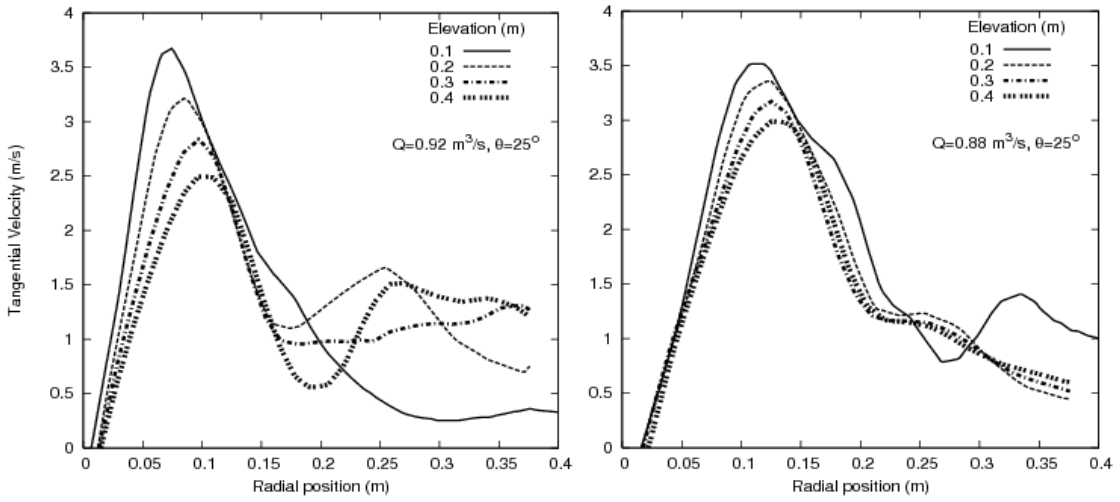

(a) Fin ratio 8.4 (fin spacing 45°) (b) Fin ratio 5.6 (fin spacing 30°)

Figure 4.5: Tangential velocity radial profiles at various elevations, for a duct width of 0.055 m and a fin angle of 25° (Note: (a) also shown in Figure 4.5 is presented here to facilitate comparison).

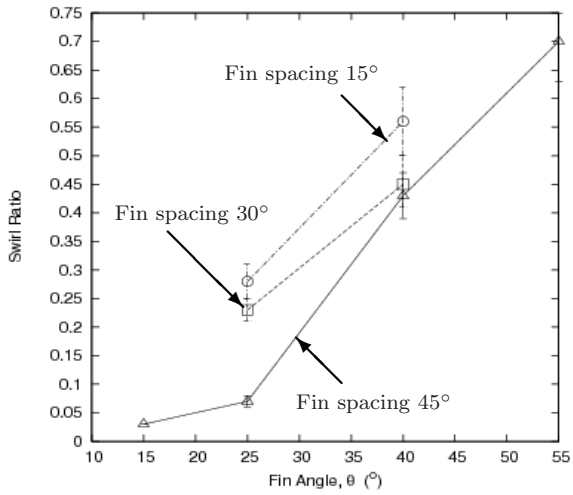

(a) Effect of swirl ratio (with estimated discretization error)

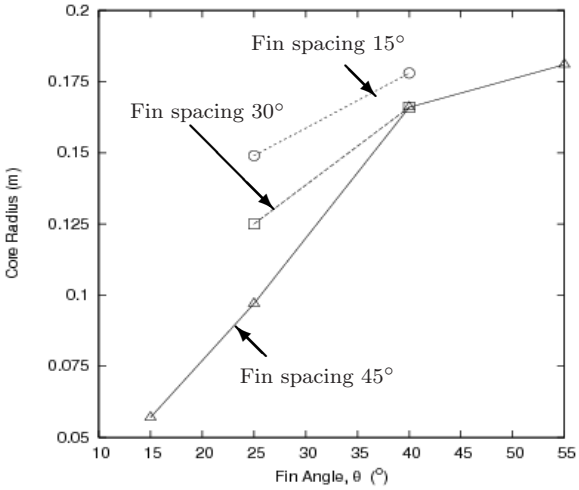

(b) Effect of core radius

Figure 4.6: Effect of the flow kinematics as a function of the fin angle for three fin spacings for a 0.055 m duct width at an elevation of 0.3 m.

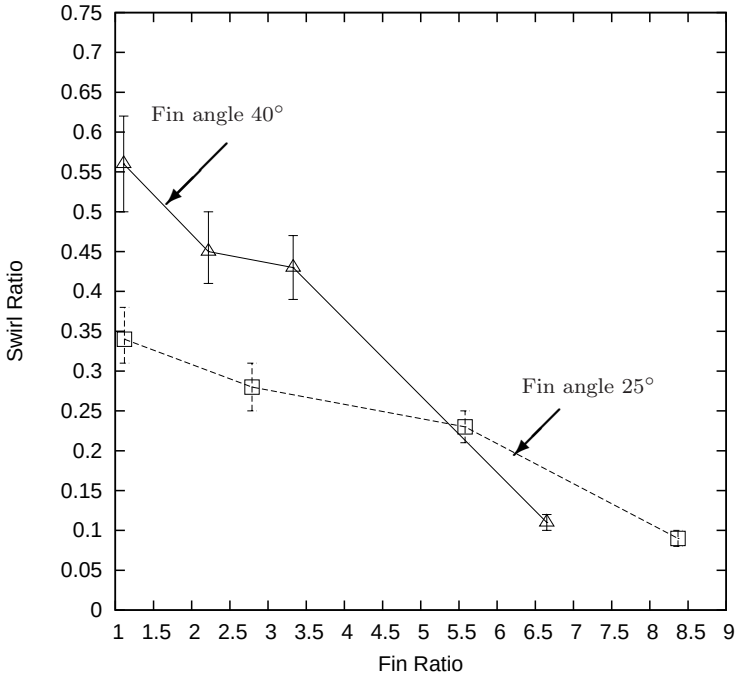

Figure 4.7: Swirl ratio (with estimated discretization error) as a function of fin ratio for two fin angles for a duct width of 0.055 m at 0.3 m elevation.

4.3 Vortex Height Sensitivity

Figure 4.8 shows the dependency of the swirl ratio, measured at an elevation of 0.3 m, on variation in vortex height with core radius shown on the secondary axis. The results show little effect on the upper boundary until the vortex height is reduced below 0.425 m. Further reductions in the vortex height results in a widening of the vortex core. The numerical model predicts that the generated vortex flow will exhibit little sensitivity to vortex height as long as the upper boundary is not reduced below some threshold value, approximately 0.425 m for the apparatus configuration considered. These results are in agreement with conclusions reported in Church et al. [1979] and Nolan and Farrell [1999].

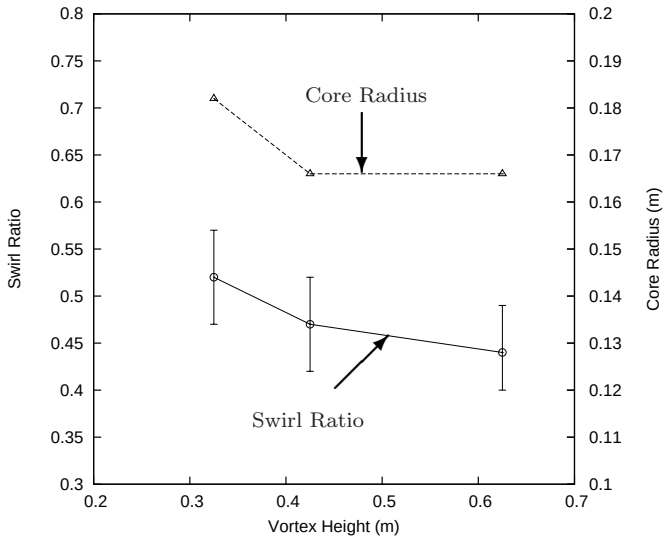

Figure 4.8: Swirl ratio (with estimated discretization error) and core radius as a function of vortex height at 0.3 m elevation.

4.4 Inflow Geometry Sensitivity

Figure 4.9 shows the swirl ratio as a function of inflow height with the core radius presented on the secondary axis. The flow exhibits little sensitivity to variations in inflow height. Comparison of the radial profile of the tangential velocity component in the vertical plane are provided in 4.10. The results show a relatively consistent vortex flow. However, some differences in the decay of tangential velocity profiles are observed particularly near the lower surface. It should be noted that the numerical predictions are obtained using an axisymmetric model. The flow characteristics may be significantly altered when a highly unsteady three-dimensional model is considered.

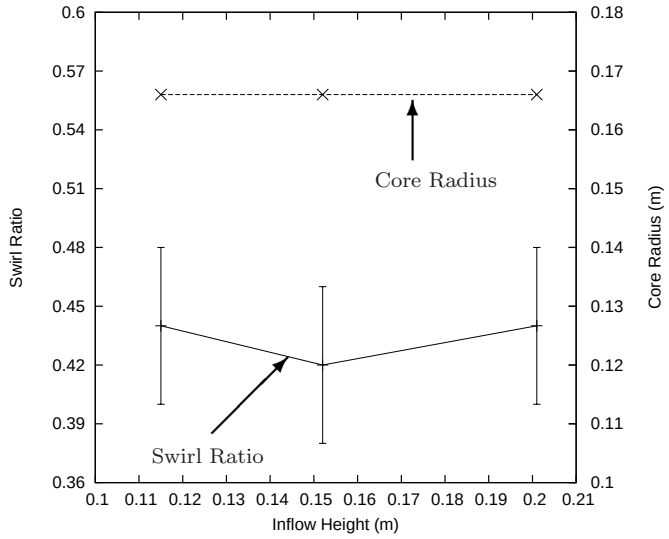

Figure 4.9: Swirl ratio (with estimated discretization error) and core radius as a function of inflow height, at an elevation of 0.3 m.

A larger inflow radii will allow a larger range of vortex flows to be generated. Previous studies (Ward [1972] and Church and Snow [1993]) have reported that as the inflow radius is reduced it becomes more difficult to generate a stable vortex flow and secondary flows can be introduced that significantly influence the vortex flow. Therefore, the inflow radius should be as large as possible to ensure that high quality vortex flows are generated.

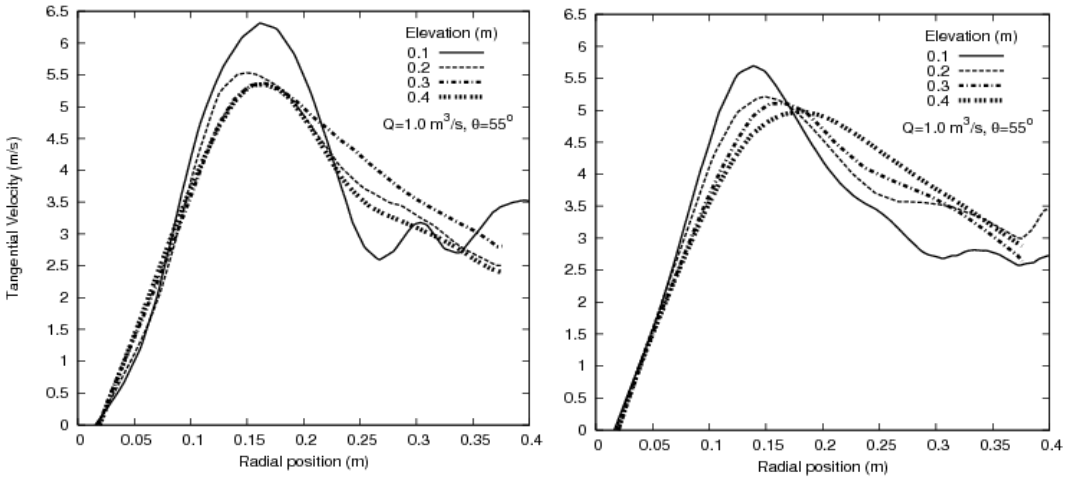

(a) Inflow height 0.115 m

(b) Inflow height 0.200 m

Figure 4.10: Tangential velocity radial profiles at various elevations

4.5 Outflow Radius Sensitivity

Figure 4.11 shows the effect that varying the outflow radius has on the core radius and the swirl ratio. As expected, the results show that the core radius scales directly with outflow radius, this agrees with previous research (D. S. Nolan and Bell [2000]). Although the core radius and swirl ratio increase, the maximum tangential velocities decrease with increasing outflow radius. The results show that the core radius increases approximately 0.75 meters per meter of increase in outflow radius. This is an important result because it demonstrates that variation of the outflow radius can be used to control the vortex flow if fin angle adjustments alone do not provide the desired vortex kinematics. It should be noted that this concept was simulated numerically for the 0.150 m outflow radius configuration. A two-dimensional slice illustrates the modification shown in Figure 4.12.

As an alternative control strategy, the fin angle can be fixed and the vortex structure controlled by varying the outflow radius. However, the results indicate the range of swirl ratios that can be generated will be significantly reduced if the vortex generator is not capable of adjusting the initial angular momentum.

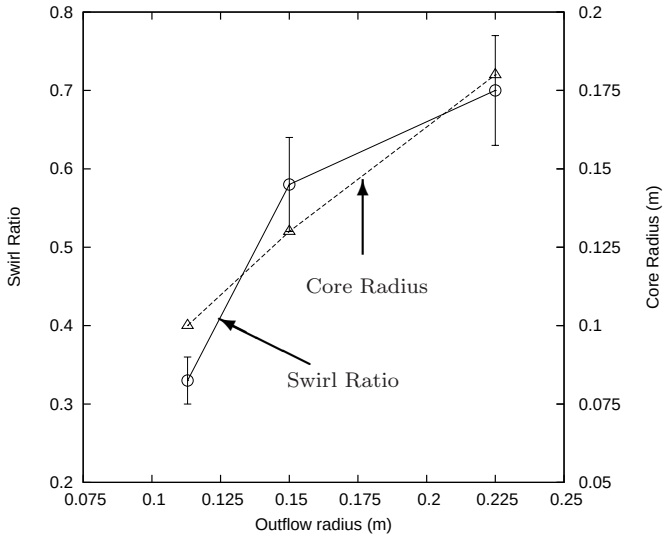

Figure 4.11: Swirl ratio (with estimated discretization error) and core radius as a function of outflow radius, for a duct width of 0.055 m at 0.3 m elevation (Note: Result at 0.15 m outflow radius uses modified outflow geometry).

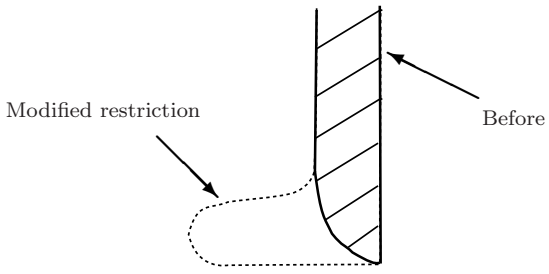

Figure 4.12: Illustration of outflow geometry modification.

4.6 Conclusions and Recommendations

The results from this sensitivity study provide information to assist in the development of an experimental vortex generator based on the design by Gallus et al. [2006] (see Figure 2.3). This sensitivity study does not attempt to model turbulence with a high level of accuracy and the wedge shaped domain modeled does not capture the highly unsteady flow expected in naturally occurring atmospheric vortex flows. These sensitivity results should only be used for providing a basis for apparatus design (see Figure 3.3 for schematic illustrating the design parameters). Further model development is required before the physical test results can be directly compared to numerical modeling results.

The vortex core flow exhibits significant sensitivity to the initial angular momentum introduced into the flow. Results from this study and previous studies (Church and Snow [1993]) show that fin surfaces that re-direct axial flow are effective at controlling the vortex kinematics. The results show that the fin angle strongly controls the initial angular momentum. However, the initial angular momentum is sensitive to several other geometric parameters consisting of the fin spacing and duct width. The numerical model predicts that the maximum vortex strength is produced when all the inlet is redirected by fin surfaces (i.e. Fin ratio=1), as originally reported in Church's review (Church and Snow [1993]). Results from this study indicate that the fin ratio should be less than some threshold value in order to ensure that a concentrated vortex flow will be generated. The duct width was also found to influence the vortex kinematics. Decreases in duct width results in smaller downdraft areas which produce higher initial angular momentum for a given flow rate. The results showed that decreasing duct width from 0.075 m to 0.055 m increased the range of vortex kinematic structures possible.

The outflow radius controls the horizontal extent of axial forcing and results show that the core radius varies in porportion to the outflow radius. Therefore, the outflow radius can be employed to control vortex kinematics. However, the range of vortex flows obtained through variation in outflow radius is significantly less than the possible range when initial angular momentum is varied.

The inflow/inlet height should be adjustable to ensure apparatus can be configured to all

planned test scenarios. The numerical results have also indicated that the vortex structure remains relatively consistent throughout the desired range of inflow/inlet heights. The apparatus geometric parameters that control flow domain, consisting of vortex height and inlet radius, should be as large as possible to minimize influence of apparatus on the vortex internal kinematic structure. The predictions from the numerical model suggest a thereshold vortex height is required to prevent significant influence on the generated flow, which is below the height restrictions imposed by the existing frame.

Results from this numerical study show that a vortex generator providing an adequate range of vortex kinematic structures can be designed to function within the confines of the existing experimental facility. To accomplish this the apparatus should allow adjustment of key geometric parameters consisting of the fin angle and outflow radius. A reduced range of vortex flows can be generated if apparatus relies only on an adjustable outflow radius. As mentioned previously the optimal apparatus geometry also requires attention to the fin ratio and duct width. Ideally the apparatus design will be capable of producing wide range of vortex structures. However, depending on apparatus construction challenges it may be preferable to accept a smaller range of fin angle adjustment with optimal fin geometry to ensure high quality vortex flows are generated. Recommendations on the range of key geometric parameters required to generate the largest range of vortex flows based on the numerical predictions are provided in Table 4.1.

Table 4.1: Geometry recommendations for the vortex generator.

Parameter description	Value
Minimum inlet radius	0.48 m
Adjustable inflow/inlet height	0.115 - 0.25 m
Outflow radius	0.10 - 0.225 m
Minimum vortex height	0.425 m
Duct width	0.055 m
Adjustable fin angle	25° to 70°
Maximum fin ratio	3.5

Chapter 5

Corner Flow Model Validation

This study is primarily concerned with the local flow kinematics of atmospheric vortices. Researchers such as Snow [1982] and Wilson and Rotunno [1982] have simplified atmospheric vortex flows into five different regions based on the governing mechanisms observed in nature. Figure 5.1 shows these regions.

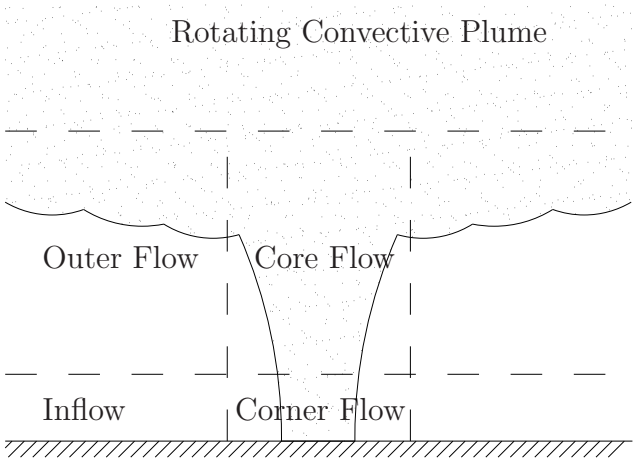

Figure 5.1: An atmospheric vortex flow simplified into five regions. Adapted from Snow [1982].

The corner flow, where the boundary layer flow transitions into the core flow, is of primary interest because this region contains the greatest pressure differentials and highest velocity gradients (Lewellen [1976]). The core radius, defined as the location of maximum tangential velocity is a governing characteristic of the flow structure near the surface (Lewellen

and Lewellen [1997]). The outer limits of this region are defined at the radial location of maximum radial velocity by some researchers (Wilson and Rotunno [1982]).

The corner and core flows are simulated using a numerical representation of a laboratory apparatus (see Figure 3.3) similar to the one developed by Gallus et al. [2006] (see Figure 2.3). This type of vortex generator is similar in some respects to the Ward apparatus and therefore, previous experimental and numerical data can be used to validate the numerical solutions. These results are also used to discuss possible flow characterization methods for highly transient vortex flows. The candidate vortex generator configuration assessed, provided in Table 5.1, is selected based on results from the sensitivity study. The following sections discuss results from three-dimensional numerical simulation using the RSM-SSG turbulence model. The improved flow predictions after considering a three-dimensional domain and employing a more representative turbulence model can also identify any weaknesses in the computationally efficient numerical model used in the sensitivity study (i.e. wedge shaped domain and $\kappa - \varepsilon$ turbulence model). It should be noted that the RSM-SSG model is based on RANS and therefore, no large-scale coherent turbulent eddies can be captured. The large-eddy simulation (LES) turbulence model directly solves for the large turbulent eddies and, for computational efficiency, employs RANS to model the smaller turbulent eddies. Lewellen and Lewellen [1997] used an LES numerical model of the corner flow region to show the importance of turbulent eddies on the maximum tangential velocities near the surface. For the present study, limitations in computational resources did not permit evaluation of a LES turbulence model.

Table 5.1: Apparatus geometry used for three-dimensional RSM-SSG model.

Parameter description	Value
Inlet radius	0.48 m
Inflow/Inlet height	0.115 m
Outflow radius	0.15 m
Vortex height	0.65 m
Duct width	0.055 m
Fin angle (θ)	55°
Fin spacing	45°
Fin ratio	1.8

Several changes in modeling set-up were employed for solution accuracy for the three-dimensional RSM-SSG model compared to the wedge shaped model used in the sensitivity study. The changes are described below (complete details are provided in Section 3.2):

- The RSM-SSG turbulence model is employed.
- A finer mesh density was used, the three-dimenisonal domain is represented using 1.6 million nodes. Computational resources did not allow a grid-independent mesh (i.e. based on the wedge domain mesh results, see Figure 3.2). However, it is believed that correct trends can be predicted using the mesh densities considered here.
- A finer time step was used (0.001s) to prevent high Courant numbers.

As expected, the solution results showed a highly transient response. Velocity components at points near the vortex core were monitored during solution to allow solution termination once the velocity exhibited a stable oscillation. Due to limitations on computational resources, the solution time range considered does not exhibit a stable oscillation. However, the solution time considered (3s to 6s) is sufficient to show that although velocity components fluctuate rapidly, the ensemble averaged velocity components changed relatively slowly. This investigation is primarily concerned with the overall flow behaviour. Therefore, the results are averaged in time and over the circumferential direction.

5.1 Discussion on Flow Kinematics and Comparison to $\kappa - \varepsilon$ Model

It is important in laboratory and numerical investigations to understand the scaling mechanism. This provides insights in the fundamental physics and allows laboratory results to be compared to naturally occurring atmospheric vortex flows. Lewellen [1962] has shown, based on the Navier-Stokes equations, that two length scales and two velocity scales can be applied to characterize a swirling sink flow. To date, the choice of scaling parameters that will allow full characterization of the corner flow region has not been agreed upon. Some researchers (D. S. Nolan and Bell [2000]) propose scaling based on the far field tangential velocity. Other researchers (Lewellen and Lewellen [1997]) recognize the importance

of the boundary layer and turbulent transport in governing the internal vortex structure and characterize flow using the internal parameters. This present study does not attempt to reconcile the various scaling methods proposed by previous researchers. Rather, the numerical results are compared to previous modeling studies using a single length and velocity scale using the following two methods: 1) scaling parameters determined at the core radius; and 2) scaling parameters based on traditional Ward apparatus parameters. Although it is known that a single length and velocity scale is insufficient to fully characterize the corner flow, research shows that it is adequate for a wide range of vortex flows. Results from the sensitivity study (as discussed in Chapter 4) provide design information for a laboratory apparatus and therefore, results presented here can be directly compared to the experimental results obtained in future work.

Figure 5.2 shows the average tangential velocity profiles at various elevations. This result shows little sensitivity in the core radius (i.e. radial location of maximum tangential velocity) and little decrease in maximum tangential velocity with increasing elevation indicating a strong vortex flow. A strong vortex flow is expected to be generated by the apparatus geometry considered.

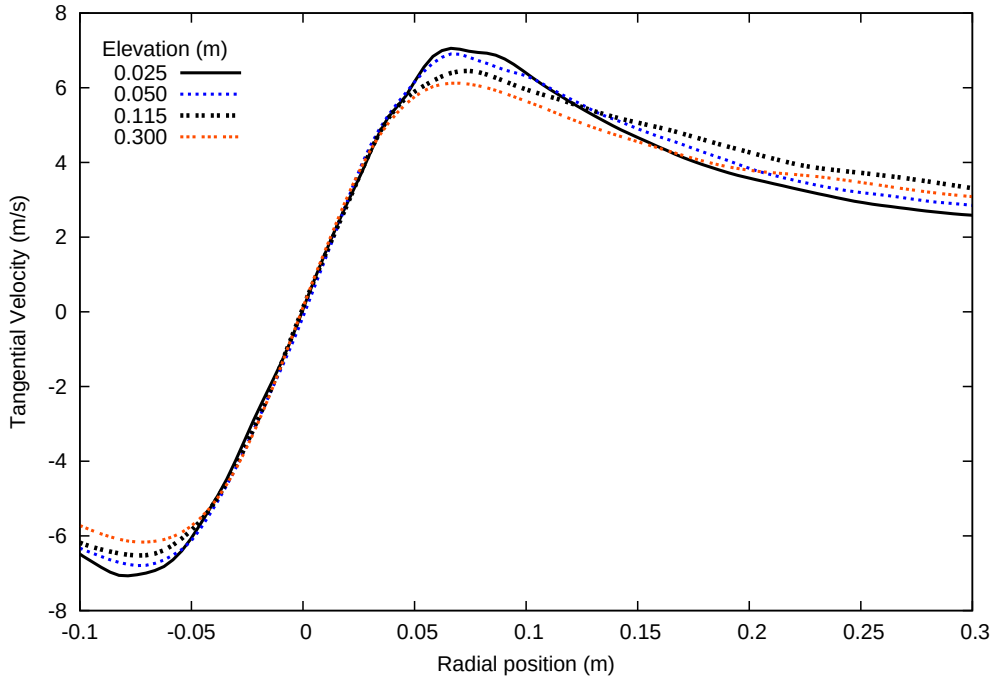

Figure 5.2: Tangential velocity profiles at various elevations.

Figure 5.3 shows the tangential velocity profiles at an elevation of 0.05 m for the RSM-SSG and the $\kappa-\varepsilon$ turbulence models for a three dimensional domain. Comparisons to numerical predictions from the $\kappa-\varepsilon$ model show significantly higher maximum tangential velocities and a smaller core radius for the RSM-SSG model. This is expected because Prieto [2006] identified that the $\kappa-\varepsilon$ model produces excessive turbulent kinetic energy at regions of high velocity gradients. As a consequence, the $\kappa-\varepsilon$ model exhibits an artificially high diffusive effect and predicts weaker velocity fields. The vortex flow parameters are presented in Table 5.2 for three numerical simulations conducted in the present study.

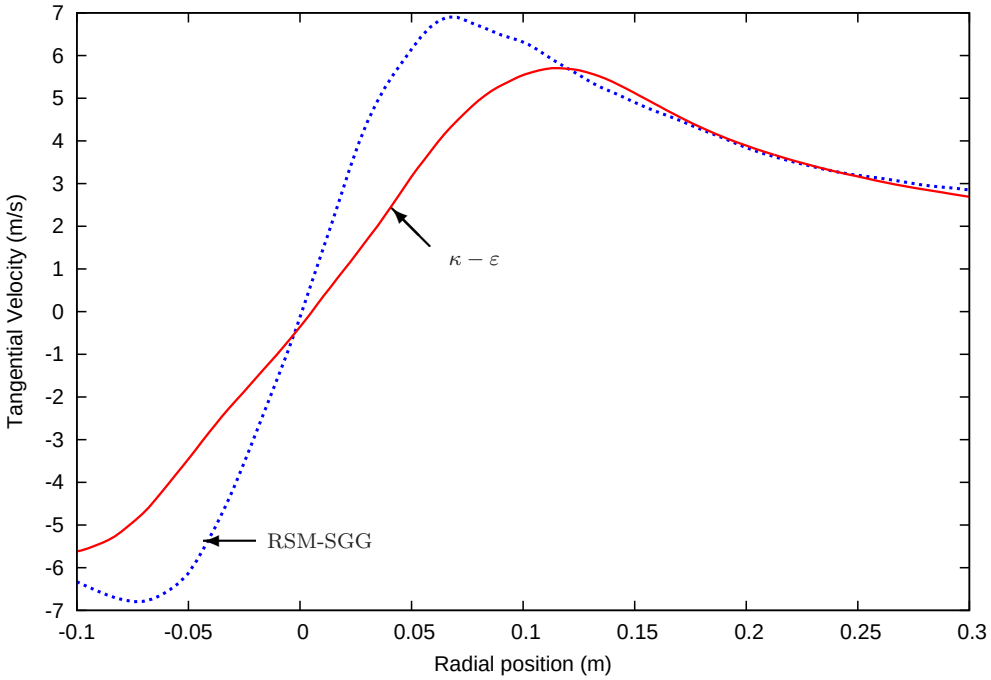

Figure 5.3: Comparison of tangential velocity profiles for RSM-SSG and $\kappa-\varepsilon$ turbulence models at a height of 0.05 m.

Table 5.2: Key corner flow parameters for numerical models of a Gallus apparatus. (elevation of 0.3 m)

Numerical model	3D RSM-SSG	3D $\kappa-\varepsilon$	Wedge $\kappa-\varepsilon$
r_{core}	0.068	0.137	0.131
S_{core}	0.16	0.60	0.58

5.2 Comparisons to Previous Modeling Studies

The Gallus vortex generator is similar to the Ward vortex generator because both apparatus simulate the inflow layer by introducing angular momentum through the use of fin surfaces and imposes convective forcing using a fan. However, the Gallus vortex generator has several major advantages including: 1) surfaces used for redirecting flow are above ground allowing translation of apparatus; and 2) does not fix the internal structure of the vortex flow.

In Prieto [2006], the vortex flow was characterized based on the geometric parameters r_0 and h. These parameters agree with the variable definitions of r_0, corresponding to the radial location of the maximum absolute radial velocity, and h, corresponding to the axial height of the maximum value of the axial velocity at r_0. For convenience, the numerical results from Prieto [2006] are presented in Figures 5.4 to 5.6 (experimental data shown from Lund and Snow [1993]).

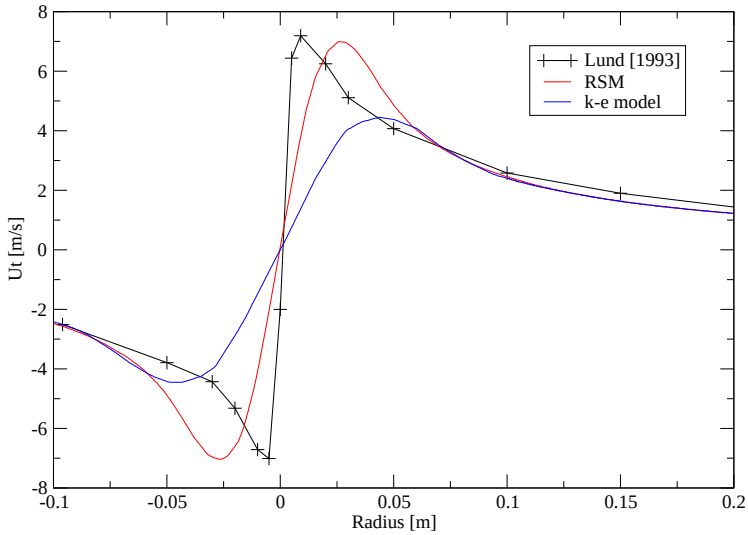

Figure 5.4: Ward's model radial profiles of the tangential velocity component at 0.15 m elevation (Prieto [2006]).

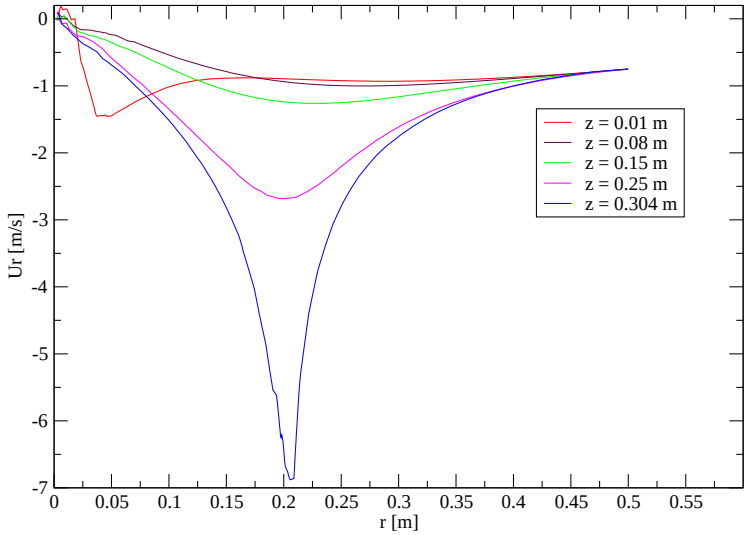

Figure 5.5: Ward's model radial profiles of radial velocity component at different elevations (Prieto [2006]).

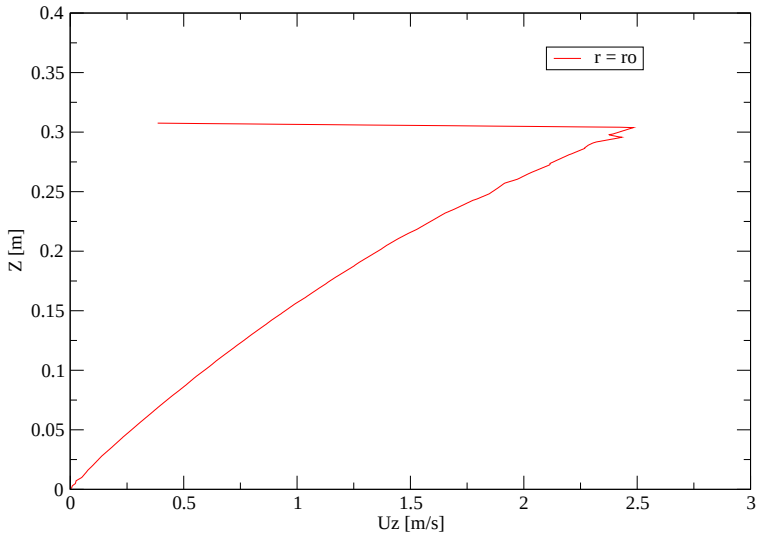

Figure 5.6: Ward's model vertical velocity component with increasing height at $r = r_0$ (Prieto [2006]).

The flow characterization described by Prieto [2006] can be modified for use with the Gallus model. Figure 5.7 shows the radial velocity component at different heights. The Gallus model numerical results for the radial velocity component is significantly different compared to the Ward model results. The primary differences include: 1) the absence of a sharp peak in radial velocity at the inflow height; 2) results show radial velocity reverses direction above the inflow height; and 3) absolute maximum radial velocity occurs near lower surface. The Gallus apparatus does not rely on an updraft hole to produce the core vortex flow, so there is no clear indication of r_0. Instead, r_0 is defined in this study as the maximum radial velocity at the inflow height (i.e. definition of h is modified for Gallus model). The flow reversal above the inlet height indicates the presence of a secondary flow which is likely influenced by the apparatus walls. This is likely to introduce inaccuracies because apparatus walls do not exist in naturally occurring vortex flows. However, the numerical results shown in Figure 5.2 predict a relatively constant core radius and a slightly decreasing maximum tangential velocity with increasing elevation. This is what is expected from previous research and therefore, these results indicate that the corner flow features of primary interest are not significantly influenced by the apparatus walls.

Figure 5.8 shows the vertical profile of the vertical velocity component at the radial location r_0. The vertical velocity also exhibits significant differences from the Ward Model. Results from the present study predict a smooth progression to the peak axial velocity and an axial location of maximum axial velocity of 0.219 m well above the inflow height.

A comparison of the radial profile of the tangential velocity component between the Gallus and Ward model was performed by scaling the Ward model numerical results (Prieto [2006]) to the numerical results generated for the Gallus apparatus. The numerical results from this study are examined at an elevation below the region where apparatus geometry is believed to influence predictions and above the region where boundary layer significantly influences the maximum tangential velocities. First, the radial location r_o was used to select a velocity scale (V^*=2.902) and length scale (L^*=1.074). Figure 5.9 shows the tangential velocity profiles for the Ward model scaled at r_o. These scaling parameters do not produce comparable vortex flows indicating that this flow characterization method may be restricted to the Ward apparatus. As an alternative, the Ward tangential velocity profile is scaled to the Gallus numerical results at the radial location of maximum tangential velocity, r_{core},

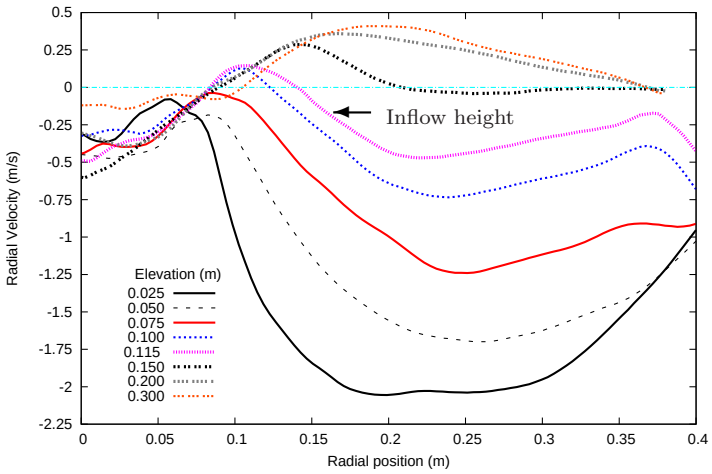

Figure 5.7: Radial profiles of radial velocity component at different elevations.

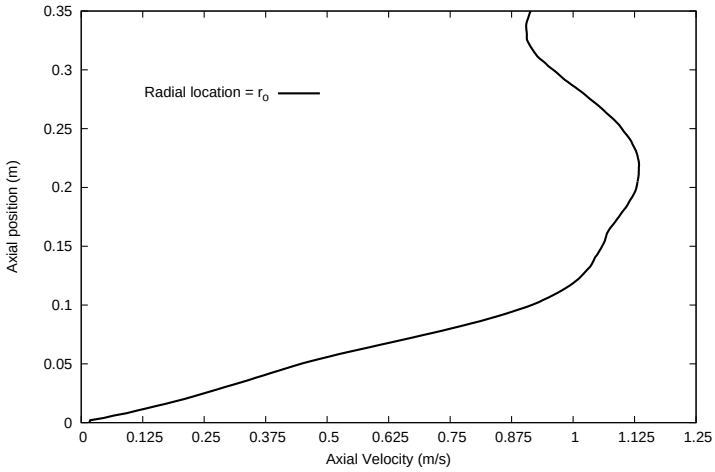

Figure 5.8: Vertical velocity component with increasing height at the radial location r_0.

shown in Figure 5.10. Comparison shows that when numerical results are scaled at the r_{core} location (velocity scale V^*=0.980 and length scale L^*=2.692) the Ward and Gallus apparatus are in reasonable agreement. This is an important result because it indicates that the generated vortex core flow is relatively insensitive to the differences in flow generation.

Figure 5.11 presents the numerical results of the tangential velocity profiles for Gallus's model compared to experimental results produced from a Gallus apparatus Sarkar et al. [2005] scaled at r_{core}. Comparison shows some differences between the experimental data and the numerical results. It is believed that the inability of the RMS-SSG turbulence model to resolve turbulent eddies leads to more diffusive vortex core flows, Lewellen and Lewellen [1997] showed the that turbulent transport of angular momentum arising from eddies intensifies the core tangential velocities. Thus, the scale is not invalid, rather it is the tangential velocity characteristic that does not match. The comparison between the experimental and RSM-SSG numerical results from Prieto's study (Figure 5.4) shows the difference expected between numerical and experimental results.

The scaling methods used in this study are not adequate to completely describe the vortex structure. However, they clearly show that the core radius provides the fundamental length and velocity scales. Although the current strategy is adequate for scaling tangential velocity profiles for comparative purposes, a more complete characterization is necessary to enhance understanding of the corner flow region. The results also show that care must be exercised when comparing experimental results to numerical results.

The numerical simulations considered in the present study generate vortex flow by redirecting axial updraft using concentric walls in a manner similar to a laboratory Gallus apparatus. It is likely that the solid walls introduce flow inaccuracies and secondary flows not present in naturally occurring atmospheric vortex flows. However, results from this study indicate that the primary flow features of interest consisting of the corner flow, specifically the maximum tangential velocity at the core radius and the near surface boundary layer, is relatively insensitive to errors introduced by the chosen vortex generating method.

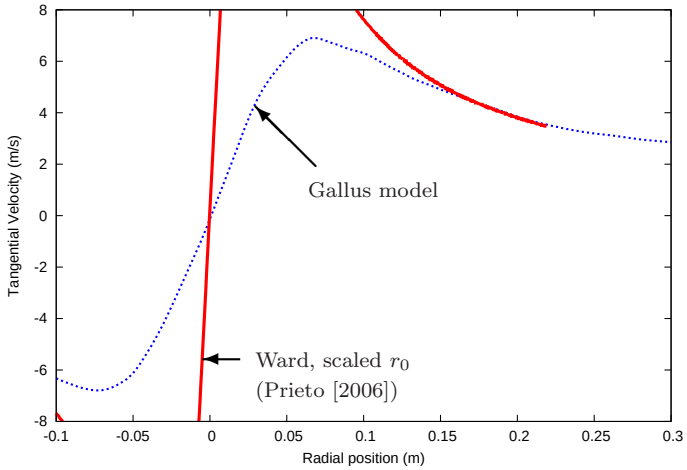

Figure 5.9: Radial profile of tangential velocity component compared to Ward's model scaled at r_0.

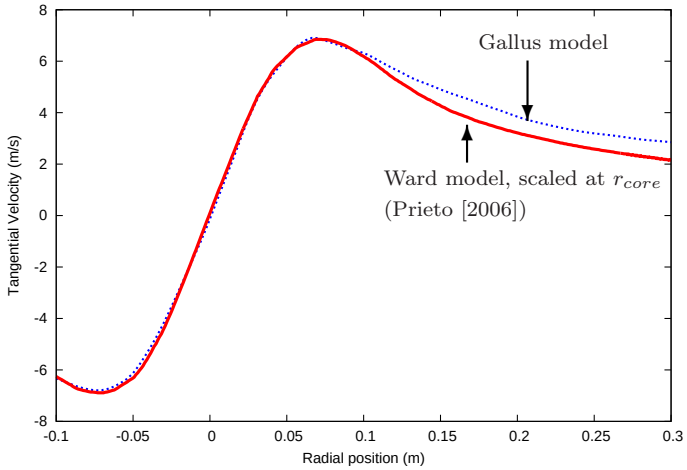

Figure 5.10: Radial profile of tangential velocity component compared to Ward's model scaled at r_{core}.

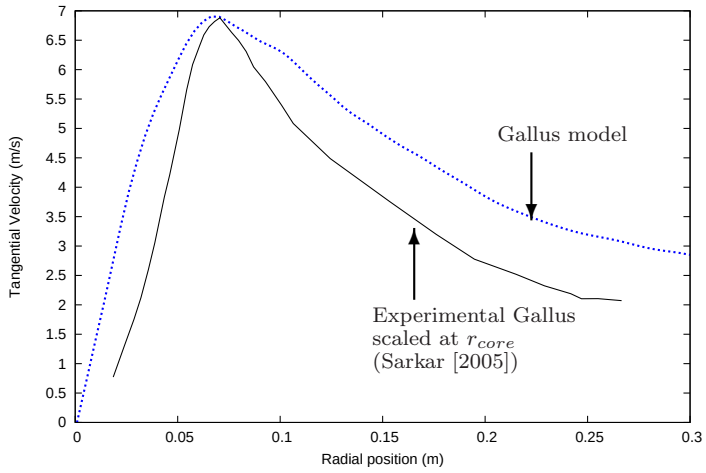

Figure 5.11: Radial profile of tangential velocity component compared to experimental Gallus result, scaled at r_{core}.

5.3 Discussion on Kinematic Characterization and Vortex Center

For vortex flows generated with a stationary apparatus the general tangential velocity profiles can be represented using either circumferential-time-averaging or just time-averaging. A comparison of the tangential velocity profiles obtained by those two averaging methods along with two instantaneous tangential velocity profiles is shown in Figure 5.12. The instantaneous tangential velocities show the vortex center moving significant distances relative to the core radius. The results indicate that time-averaged results on a single vertical plane can sufficiently describe the general tangential velocity. It is likely that better agreement would result if averaging is performed using a finer time resolution over a larger time range.

Although the averaged results show the vortex center approximately corresponds to the apparatus center for the stationary apparatus considered here, a method for evaluating the center location is necessary when considering a translating vortex flow. It is believed that the radial profile of the pressure differential can be used to determine the vortex center. The radial profile of pressure differential is governed by the inverse square of the radial distance from the vortex center (Ward [1972]). Figure 5.13 shows radial profiles

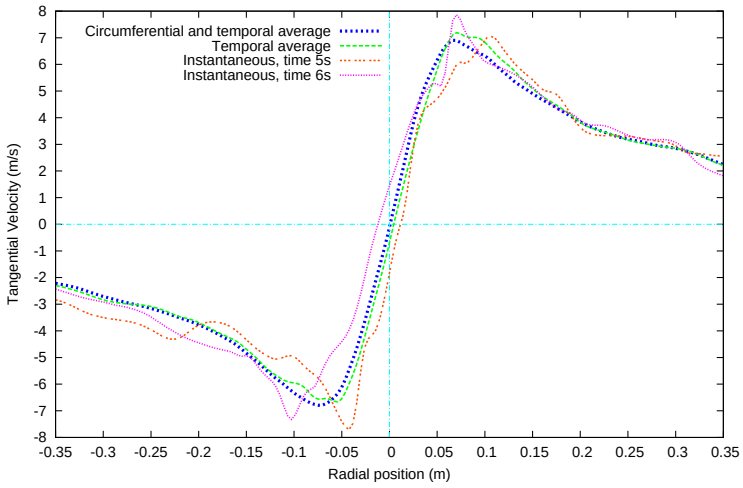

Figure 5.12: Radial profile of tangential velocity component for two averaging techniques along with two instantaneous profiles at an elevation of 0.05 m.

of pressure differential for two averaging techniques along with two instantaneous profiles. The vortex center predicted using the minimum pressure differential corresponds to the center determined using the tangential velocity and therefore, the results show the vortex core center can be predicted using radial profiles of the tangential velocity or pressure differential. However, this methodology assumes the radial profile intersecting the vortex center is known.

In some experiments the velocity magnitude is more readily measured than the velocity components. The velocity magnitude is also a scalar quantity independent of the location of the vortex center. Figure 5.14 shows radial profiles of the velocity components with the velocity magnitude. These results indicate that the minimum velocity magnitude corresponds to the vortex center. For the flow configuration considered the velocity magnitude is similar to the tangential velocity within the core due to the relatively small axial and radial components indicating that the velocity magnitude can also approximate the location of core radius. The sharp gradients exhibited by the velocity magnitude make it preferable for determining the vortex center compared to the pressure differential profile. Figure 5.15 shows contours depicting the velocity magnitude on a horizontal plane (elevation of 0.5 m) at two instances. This comparison shows movement of the vortex center with time and also

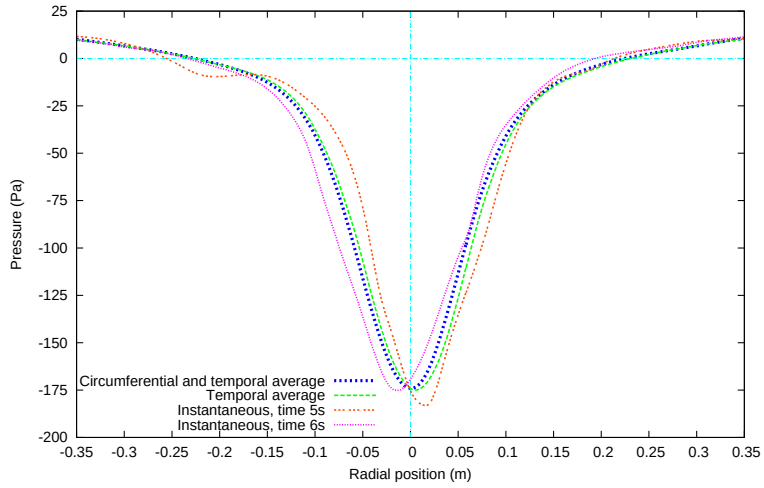

Figure 5.13: Radial profile of pressure differential for two averaging techniques along with two instantaneous profiles at an elevation of 0.05 m.

shows the transient nature of this flow.

The following basis is suggested for evaluating the center of the vortex core on a horizontal plane.

$$U_{center} = min(\mid \mathbf{u} \mid) \tag{5.1}$$

where $\mid \mathbf{u} \mid$ is the velocity magnitude and U_{center} is the minimum instantaneous velocity over the region considered. To determine the center location a horizontal plane is selected, then the position of U_{center} corresponds to the center location on the plane selected. The time-averaged center ($\bar{U}_{center}$) can then be calculated using the instantaneous centers. Figure 5.16 shows the positions of the instantaneous vortex core centers on the horizontal plane along with the time-averaged center.

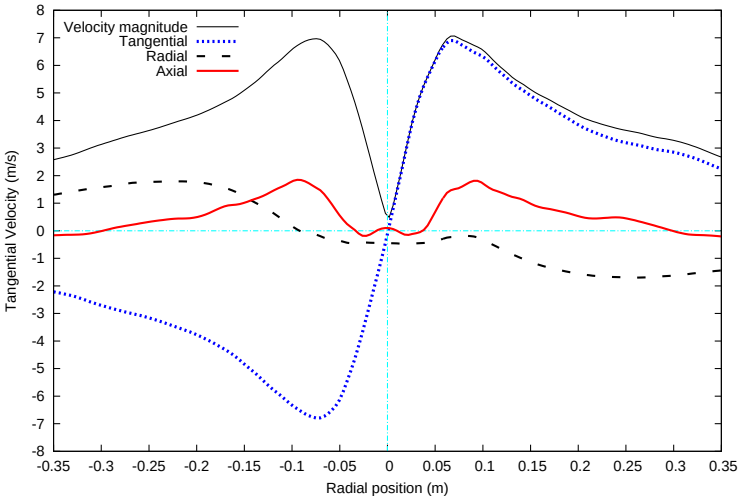

Figure 5.14: Radial profiles of the velocity magnitude and velocity components at an elevation of 0.05 m.

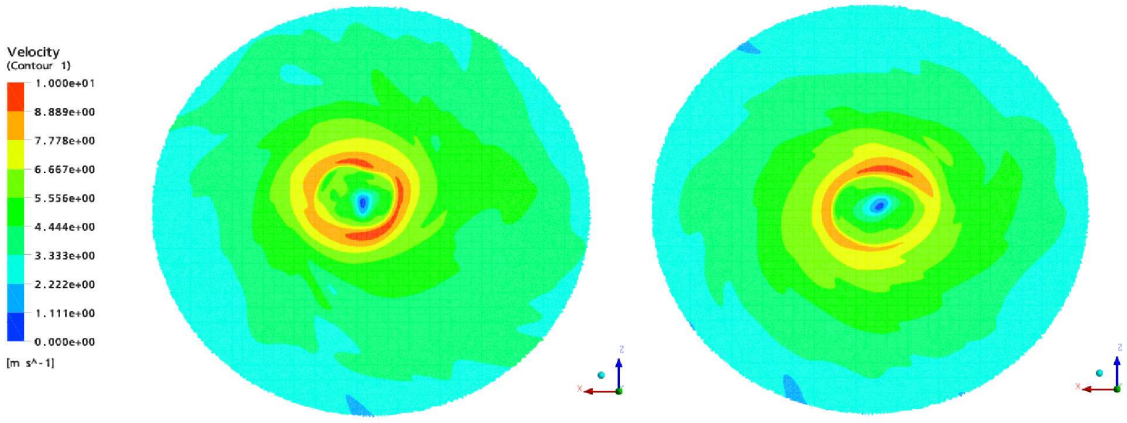

(a) time=5s (b) time=6s

Figure 5.15: Contours of the instantaneous velocity magnitude on a horizontal plane at an elevation of 0.05 m.

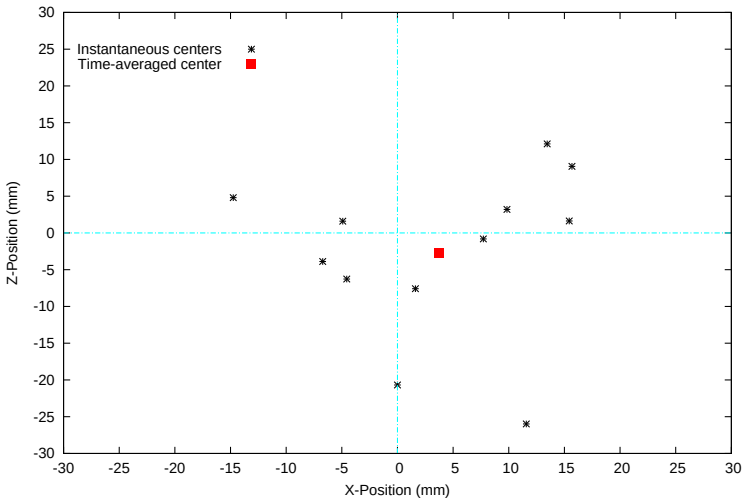

Figure 5.16: Instantaneous position of core vortex center on horizontal plane at an elevation of 0.05 m, time resolution 0.25s.

5.4 Conclusions

The suitability of several turbulence models, $\kappa - \varepsilon$ and RSM-SSG models, is considered by comparing previous experimental and numerical Ward results to numerical predictions of vortex flows generated by a Gallus apparatus. The results agree with previous research (Prieto [2006]) and show that the RSM-SSG turbulence model is in better agreement with experimental data. However, the RSM-SSG turbulence model exhibits a diffusive influence likely due to an inability to resolve large-scale turbulent eddies. As a consequence the RSM-SGG numerical model predicts a weaker velocity field in the vortex core region compared to experimental results. Thus, care must be excercised when investigating naturally occurring atmospheric vortex flows using numerical simulations employing the RSM-SSG turbulence model.

To validate the numerical Gallus model comparisons were made using previous results of a Ward apparutus. The Ward results scaled using parameters traditional to Ward modeling studies (r_0) did not agree with the numerical results for the Gallus apparatus. The fundamental length and velocity scales correspond to the radial location of the maximum tangential velocity (i.e. core radius, r_{core}). Scaling parameters determined using the core

radius show the tangential velocities generated from the previous Ward modeling studies reasonably agree with results from the present study modeling a Gallus apparatus. Although it is known that a single velocity scale and length scale are inadequate to fully characterize the corner flow region research shows it can adequately capture the salient flow behaviour for a wide range of vortex flow configurations.

Vortex flows generated by the Gallus apparatus are preferable because the internal vortex structure is not fixed. As a consequence, radial and axial velocity profiles do not exhibit the sharp gradients near the location of maximum radial velocity as observed in flows produced by the Ward apparatus. The results clearly show similar vortex core structures can be generated using either the Ward or Gallus vortex apparatus, indicating that the kinematic structure is relatively insensitive to errors introduced from the laboratory apparatus. However, it is likely that artificial flow features exist as a result of the solid walls used to redirect flow. These inaccuracies are accepted because they are shown to have little influence on the internal vortex structure (i.e. corner flow region). In future studies, similar numerical models will be employed to study mass transport of water vapour in the corner flow region. In these studies, the influence of solid walls and the artificial downdraft produced by the Gallus apparatus should be considered. In addition, it would be useful to confirm the present results with finer mesh commensurate with grid independence.

Results from the three-dimensional RSM-SSG model show a highly transient response. The results show that for a stationary apparatus the general flow response can be captured by time-averaging on a single vertical plane. It is more difficult to extract the vortex flow when a translating vortex is considered. In this case the location of vortex center can be used to extract the vortex flow from the translating and swirling flow. Results show the vortex center location can be determined using either the velocity magnitude or pressure. In this study the velocity magnitude is preferable because it exhibits a more pronounced minima.

Bibliography

G. R. B. E Launder and W. Rodi. Progress in the developments of a reynolds-stress turbulence closure. *J. Fluid Mechanics*, 68:537 – 566, 1975.

C. R. Church and J. T. Snow. *The Tornado: Its Structure, Dynamics, Prediction, and Hazards*, chapter Laboratory Models of Tornadoes, pages 277 – 295. American Geophysical Union, Washington, D. C., USA, 1993.

C. R. Church, J. Snow, G. Baker, and E. M. Agee. Characteristics of tornado-like vortices as a function of swirl ratio: A laboratory investigation. *J. Atmos. Sci.*, 36:1755 – 1776, 1979.

S. A. D. S. Nolan and J. Bell. Studies of the relationship between environmental forcing and the structure and dynamics of tornado-like vortices. *Lawrence Berkeley National Laboratory*, pages 1 – 65, 2000.

R. P. Davies-Jones. The dependence of core radius on swirl ratio in a tornado simulator. *J. Atmos. Sci.*, 30:1427 – 1430, 1973.

R. P. Davies-Jones. Laboratory simulations of tornadoes. *Preprints Symposium on Tornadoes*, pages 151 – 174, 1976.

W. A. Gallus, F. L. Haan, P. P. Sarkar, K. Le, and J. Wurman. Comparison of numerical model and laboratory simulator tornado wind fields with radar observations of the Spencer, South Dakota tornado. In *Symposium on the Challenges of Severe Convective Storms*, Atlanta, GA, USA, 2006. Amer. Meteor. Soc.

R. Greeley, J. Iversen, G. Beardmore, B. Mickelson, and S. Metzger. Martian dust devils: Laboratory simulations. In *XXXII Lunar and Planetary Science*, 2001.

P. Howells, R. Rotunno, and R. Smith. A comparative study of atmospheric and laboratory-analogue numerical tornado-vortex models. *Q. J. R. Meteorol. Soc.*, 114:801 – 822, 1988.

A. Kolmogorov. Dissipation of energy in the locally isotropic turbulence. *Dokl. Akad. Nauk. SSSR*, 30(301), 1941. Reprinted in Proc. R. Soc., London, 1991.

B. E. Launder and D. Spalding. The numerical computation of turbulent flows. *Comput. Methods Appl. Mech. Eng.*, 3:269 – 289, 1974.

D. C. Lewellen and W. S. Lewellen. The influence of local swirl ratio on tornado intesification near the surface. *J. Atmos. Sci.*, 57:527 – 544, 2000.

W. S. Lewellen. A solution for three-dimensional vortex flows with strong circulation. *J. Fluid. Mech.*, 14:420 – 432, 1962.

W. S. Lewellen. Theoretical models of the tornado vortex. In R. E. Peterson, editor, *Proceedings of Symposium on Tornadoes*, pages 107 – 143, Lubbock, Texas, USA, 1976. Texas Tech. University.

W. S. Lewellen and D. C. Lewellen. Large-eddy simulation of a tornado's interaction with the surface. *J. Atmos. Sci.*, 54(5):581 – 605, 1997.

D. E. Lund and J. T. Snow. *The Tornado: Its Structure, Dynamics, Prediction, and Hazards*, chapter Laser Doppler Velocimeter Measurements in Tornadolike Vortices, pages 297 – 306. American Geophysical Union, Washington, D. C., USA, 1993.

S. M. Metzger, J. R. Johnson, J. R. Carr, T. J. Parker, and M. T. Lemmon. Dust devils vortices seen by the Mars Pathfinder Camera. *Geophys. Res. Lett.*, 26:2781 – 2784, 1999.

D. S. Nolan and B. F. Farrell. The structure and dynamics of tornado-like vortices. *J. Atmos. Sci.*, 56:2908 – 2936, 1999.

S. B. Pope. *Turbulent Flows*. Cambridge University Press, 2000.

L. Prieto. A numerical model of local water vapour transport. pages 1 – 105, 2006.

R. Rotunno. Numerical simulation of a laboratory vortex. *J. Atmos. Sci.*, 34:1942 – 1956, 1977.

R. Rotunno. A study in tornado-like vortex dynamics. *J. Atmos. Sci.*, 36:140 – 152, 1979.

P. P. Sarkar, F. L. Haan, W. A. Gallus, K. Le, and J. Wurman. Velocity measurements in a laboratory tornado simulator and their comparison with numerical and full-scale data. In *Proceedings of the 37th joint meeting with the panel on wind and seismic effects*, 2005.

J. T. Snow. A review of recent advances in tornado vortex dynamics. *Rev. Geophy. Space Phys.*, 20(4):953 – 964, 1982.

C. G. Speziale, S. Sarkar, and T. B. Gatski. Modelling the pressure-strain correlation o turbulence: An invariant dynamical system approach. *J. Fluid. Mech.*, 227:245 – 272, 1991.

P. Thomas and P. J. Gierasch. Dust devils on Mars. *Science*, 230:175 – 177, 1985.

N. B. Ward. The exploration of certain features of tornado dynamics using a laboratory model. *J. Atmos. Sci.*, 29:1194 – 1204, 1972.

T. Wilson and R. Rotunno. Numerical simulation of a laminar vortex flow. In *Proceedings of International Conference on Computational Methods and Experimental Measurements*, Washington, D. C., USA, 1982. ISCME.

Y. Z. Zhao, Z. L. Gu, Y. Z. Yu, Y. Ge, Y. Li, and X. Feng. Mechanism and large eddy simulation of dust devils. *Atmosphere-Ocean*, 42(1):61 – 84, 2004.